

# **PRODUCTION AND CHARACTERIZATION OF NOVEL CHEMOKINE DECOY PROTEINS**

**Tatjana Hana Dittrich**

**A Thesis  
Submitted in Partial Fulfilment of the  
Requirements for the Degree of**

**MASTER OF SCIENCE**

**In**

**Biochemistry and Molecular Biomedicine  
Institute of Biochemistry**

**University of Technology  
Graz, Austria**

**April 2013**

**Thesis Advisor at the Technical University:  
Univ.-Prof. Dr. rer. nat. Peter Macheroux  
Institute of Biochemistry**

**Thesis Advisor at ProtAffin:  
Univ.-Prof. Mag. Dr.rer.nat. Andreas Kungl**

## **ACKNOWLEDGEMENTS**

*The experimental part of the thesis has been carried out at the ProtAffin Biotech Company in Graz.*

*My gratitude goes to my thesis advisor Prof. Dr. Andreas Kungl for his help and collaboration. I also like to express my deep gratitude for the opportunity to join the team of ProtAffin and to be part of their research.*

*My special thanks goes to my thesis co-advisor, Dr. Daniela Schweiger.*

*I would also like to express my gratitude to my advisor at the university, Prof. Dr. Peter Macheroux for his help, for his friendly attitude and especially for his excellent biochemistry lectures.*

*I would also like to thank Dr. Martina Theuer for her advice and help with the huge amounts of data we collected.*

*I also like to thank the whole team of ProtAffin for their help.*

*And last but not least I would like to thank my parents and friends for their constant support.*

# TABLE OF CONTENTS

ACKNOWLEDGEMENTS.....	2
TABLE OF FIGURES .....	5
LIST OF TABLES .....	7
ABBREVIATIONS .....	9
OBJECTIVES OF WORK.....	11
1. Abstract.....	12
2. Zusammenfassung.....	13
3. Introduction .....	14
3.1 Chemokines.....	14
3.1.1 Classification of Chemokines.....	14
3.1.2 Basic Structure .....	15
3.1.3 Chemokine Receptors .....	15
3.1.4 Chemokine function .....	15
3.2 The role of chemokines in pathology .....	16
3.2.1 Role of chemokines in Multiple Sclerosis (MS) .....	16
3.2.2 Role of chemokines in Arthritis.....	17
3.2.3 Role of chemokines in COPD (chronic obstructive pulmonary disease) .....	18
3.2.4 Role of chemokines in neoplastic processes.....	19
3.3 Glycosaminoglycans (GAG).....	20
3.3.1 Proteoglycans (PG) .....	21
3.3.2 Chemokine - GAG interactions .....	22
3.4 Description of MCP-1.....	23
3.5 Description of IL-8.....	24
3.6 Glycan-binding decoy proteins - CellJammer™ .....	25
4. Materials and Methods .....	25
4.2 Chemicals.....	25
4.3 Chromatography columns and resins.....	26
4.4 Antibodies.....	26
4.5 Reference proteins .....	27
4.6 GAGs.....	27
4.7 Cell culture .....	27

4.8	Bifunctionals sequence overview .....	28
4.9	Fermentation and Expression Analysis .....	29
4.10	Purification of bifunctional proteins (PA1113 – PA1118) .....	30
4.10.1	Cell disruption, inclusion body (IB) solubilisation and dialysis .....	30
4.10.2	1 <sup>st</sup> purification step: cation exchange chromatography.....	31
4.10.3	2 <sup>nd</sup> purification step: reversed phase HPLC .....	31
4.10.4	3 <sup>rd</sup> purification step: cation exchange chromatography, refold and dialysis .....	32
4.11	Biophysical characterization of the purified bifunctional proteins.....	33
4.11.1	Determination of protein concentration of the bifunctionals.....	33
4.11.2	Confirmation of purity and identity of purified proteins by SDS PAGE (Sodium Dodecyl Sulfate Polyacrylamide Gel Electrophoresis).....	34
4.11.3	Confirmation of identity and quality of purified bifunctionals by Mass spectrometry	34
4.11.4	Limulus amoebocyte lysate (LAL) Test .....	35
4.11.5	Determination of Protein Fold by Guanidine Unfolding and Fluorescence Shift...35	
4.11.6	Determination of secondary structure by Far-UV-Circular Dichroism Spectroscopy (CD spectroscopy) .....	36
4.11.7	Determination of the affinity to immobilised GAGs by Surface Plasmon Resonance (SPR).....	37
4.11.8	Determination of affinity to GAGs by Isothermal fluorescence titration (IFT) .....	38
4.11.9	Determination of affinity to GAGs by Isothermal Titration Calorimetry (ITC).....	38
4.11.10	Determination of MW and Oligomerisation Behaviour by Size Exclusion Chromatography (SEC) .....	39
4.11.11	Determination of MW and Oligomerisation Behaviour by Anisotropy Measurements.....	39
4.11.12	Boyden chamber assay .....	41
5.	Results and Discussion .....	41
5.2	Fermentation and expression analysis.....	41
5.3	Purification of bifunctional proteins (PA1113 – PA1118) .....	42
5.4	Biophysical characterization of proteins .....	43
5.4.1	Confirmation of Purity and Identity of purified proteins by SDS-PAGE .....	43
5.4.2	Confirmation of identity and quality of purified bifunctionals by Mass spectrometry	45
5.4.3	Limulus amoebocyte lysate (LAL) Test .....	46
5.4.4	Determination of protein folding by guanidine unfolding and fluorescence shift...46	
5.4.5	Determination of secondary structure by Far-UV-Circular Dichroism Spectroscopy (CD spectroscopy) .....	49
5.4.6	Determination of affinity to GAGs by Surface Plasmon Resonance (SPR).....	51
5.4.7	Determination of affinity to GAGs by Isothermal fluorescence titration (IFT) .....	52
5.4.8	Determination of Affinity To GAGs By Isothermal Titration Calorimetry (ITC).....	54
5.4.9	Determination of MW by Size Exclusion Chromatography (SEC).....	55
5.4.10	Boyden Chamber Assay .....	56
6.	Conclusion .....	58
7.	References.....	60

## TABLE OF FIGURES

Figure 1: Structure of the major disaccharide repeating unit of heparin (38).....	20
Figure 2: Structure of the major disaccharide repeating unit in heparan sulfate (38).....	20
Figure 3: Structure of glypicans and syndecans (45).....	22
Figure 4: Shows the schematic representation of the CCL2 domain structure. (8).....	24
Figure 5: pJexpress411 vector from DNA2.0 .....	28
Figure 6: Graphic representation of the elution gradient.....	32
Figure 7: CD spectra standard obtained from <a href="http://www.ap-lab.com/circular_dichroism.htm">http://www.ap-lab.com/circular_dichroism.htm</a> .....	36
Figure 8: Expression analysis of PA1113 – PA1115 by SDS-PAGE and Coomassie staining before induction and after one to four hours. Red arrows indicating the anticipated protein band after induction of expression.....	42
Figure 9: Expression analysis of PA1116-PA1118 by SDS-PAGE and Coomassie staining before induction and after one to four hours. Red arrows indicating the anticipated protein band after induction of expression.....	42
Figure 10: SDS PAGE analysis and Silver stain of purified bifunctionals PA1113 – PA1118.	44
Figure 11: Western blot of purified bifunctionals PA1113 – PA1118 performed with IL-8 antibody (Szabo Scandic) .....	44
Figure 12: Silver stain of all 6 bifunctionals. The spots were excised and used for the MS/MS analysis. ....	45

Figure 13: A fluorescence shift experiment using the example of PA1115 B001.....	47
Figure 14: A fluorescence shift experiment using the example of PA1115 B001 with all concentrations.....	48
Figure 15: A guanidine unfolding experiment using the example of PA1115 B001 .....	49
Figure 16: Overlay of the recorded spectra of PA113, PA1116, PA1117 and PA1118 in the absence of heparin.....	50
Figure 17: Overlay of the recorded spectra of PA113, PA1116, PA1117 and PA1118 in the presence of heparin.....	50
Figure 18: An exemplary sensorgram of PA401.....	51
Figure 19: Overlay of all performed IFTs. The normalized change in fluorescence is plotted against the concentration of added ligand. The results of the titration with heparin are shown in the upper chart, whereas the results of the titration with heparan sulfate as ligand are shown in the lower chart.....	54
Figure 20: An exemplary ITC measurement showing the spikes in heat flow upon ligand injection in the upper part. The lower part shows the corresponding spectra after peak integration and plotted as a function of the molar ratio between the free ligand and the complex.....	55
Figure 21: Summarized results of SEC analysis of PA1113-PA1118. The absorbance [mAU] is plotted against the retention time [min]. .....	56
Figure 22: Pictures of neutrophil cells after the performed boyden chamber assay. a) PA1115 13 nM b) PA1115 130 nM c) PA1115 1300 nM d) background with PBS .....	57
Figure 23: Pictures of neutrophil cells after the performed boyden chamber assay. a) IL-8 wt 13 nM b) IL-8 wt 130 nM c) IL-8 wt 1300 nM d) background with PBS.....	58

## LIST OF TABLES

Table 1: Overview of bifunctional protein sequences .....	28
Table 2: Gradient used in the rpHPLC step.....	31
Table 3: Settings for Record of Fluorescence Spectra .....	35
Table 4: Settings for CD spectroscopy.....	36
Table 5: SPR settings .....	37
Table 6: Bifunctional dilutions in PBST .....	37
Table 7: Isothermal Titration Calorimetry- Parameters.....	39
Table 8: Settings for Anisotropy measurements.....	40
Table 9: Summarized results of the MS/MS analysis (PA1113-PA1118).....	46
Table 10: Results of all fluorescence shift experiments in PBS and in 6 M Gdn-HCl.....	47
Table 11: Result summary of the Gdn-HCl unfolding experiments.....	48
Table 12: Results of measurements on a C1 chip .....	51
Table 13: Results of measurements on a SA-chip .....	52
Table 14: Summarized results of all performed measurements with heparin (Iduron BN3) as ligand .....	52
Table 15: Summarized results of all performed measurements with heparan sulfate (Iduron BN1) as ligand.....	53

Table 16: Summary of performed ITC measurements of PA1113-PA1118 ..... 55

Table 17: Summarized results of the SEC analysis of PA1114-PA1118 as well as the  
calculated results for the MW. .... 56

## ABBREVIATIONS

aa	amino acids
ACN	Acetonitrile
autofluorescence	Automatic isothermal fluorescence titration
BCA	Bicinchoninic acid
b-GAG	Biotinylated glycosaminoglycan
b-Hep	Biotinylated heparin
b-HS	Biotinylated heparan sulfate
BM	Basement membrane
CD	Circular dichroism
COPD	Chronic obstructive pulmonary disease
Da	Dalton
DS	Dermatan sulfate
ECM	Extracellular matrix
<i>E.coli</i>	Escherichia coli
FSB	Final sample buffer
FPLC	Fast performance liquid chromatography
GAG	Glycosaminoglycan
Hep	Heparin
HIC	Hydrophilic interaction chromatography
HPLC	High pressure liquid chromatography
HS	Heparan sulfate
HSPG	Heparan sulfate proteoglycan
IB	Inclusion body
IFT	Isothermal fluorescence titration
IL-8	Interleukin 8
IPTG	Isopropyl $\beta$ -D-1-thiogalactopyranoside
ITC	Isothermal titration calorimetry
Kd	Dissociation constant
kDa	Kilo Dalton
LAL	Limulus amoebocyte lysate
MCP-1	Monocyte chemoattractant protein-1
MHS	Macroprep High S
MRE	Mean residue ellipticity
MS	Mass spectrometry
MS	Multiple Sclerosis
MW	Molecular weight
NaCl	Sodium chloride
NaOH	Sodium hydroxide
NSCLC	non-small cell lung carcinoma
ONC	Over-night culture
PA	Polyacrylamide
PAGE	Polyacrylamide gel electrophoresis
PBS	Phosphate buffered saline
PTM	Posttranslational modification
rpHPLC	Reversed phase high performance liquid chromatography
SB	SeeBlue 2 Plus Protein Marker
SDS PAGE	Sodium dodecyl sulphate polyacrylamide gel electrophoresis
SP sepharose	Sulfopropyl sepharose
SPFF	Sulfopropyl sepharose fast flow

SPR  
TFA  
WCW  
wT

Surface plasmon resonance  
Trifluoroacetic acid  
Wet cell weight  
Wild type

## OBJECTIVES OF WORK

The main objective of our work was to generate new fusion decoy proteins, composed of an IL-8 mutant (PA401) and a MCP-1 mutant (PA508) with an enhanced binding affinity to GAGs but impaired binding ability to the IL-8 and MCP-1 receptor. The second objective was the production of the fusion proteins in sufficient amounts for testing purposes and their characterization via biophysical methods.

Our work included the following steps:

- ❖ Recombinant production of the new fusion proteins in *E.coli*.
  
- ❖ Purification of the proteins via chromatographic techniques and optimization of the purification protocol to maximize protein yield.
  
- ❖ Characterization of fusion proteins to ensure the purity and identity by SDS-PAGE, isothermal fluorescence titration (IFT), size exclusion chromatography (SEC), and mass spectroscopy (MS).
  
- ❖ Identification of secondary structures and affinity by surface plasmon resonance spectroscopy (SPR), CD spectroscopy and isothermal titration calorimetry (ITC).
  
- ❖ The performance of a cell-based assay (Boyden chamber) to ensure the impaired receptor binding resulting in reduced chemotactic activity.

## **1. ABSTRACT**

The present master thesis describes results of experiments to obtain therapeutically promising modified chemokines.

Chemokines are a class of small chemotactic cytokines which are involved in a variety of normal physiological but also pathological processes in the human body. Because of their major role, chemokines have been associated with several pathological conditions, mainly autoimmune and inflammatory diseases like COPD and arthritis. As it became apparent that the recruitment of inflammatory cells to the inflammation site is greatly influenced by the interaction between chemokines and glycosaminoglycans, this particular interaction poses a potential target for treating inflammatory processes.

This approach theoretically circumvents limitations and problems of small molecule inhibitors and antibody treatments.

ProtAffin is a biotechnology company investigating the therapeutic potential of glycan-binding decoy proteins and has developed a strong pipeline of dominant-negative chemokine variants. The working hypothesis of the current experiments was to test, whether a combination of modified chemokines is more efficacious than the single mutant molecule or exhibits different biological effects.

Six different products were obtained in satisfactory purity and in a yield that allowed a complete chemical characterization. Further experiments in biological systems are envisaged to test the biological activity in pharmacological models of inflammation.

## **2. ZUSAMMENFASSUNG**

Die vorliegende Masterarbeit beschreibt die Ergebnisse von Experimenten, mit denen modifizierte Chemokine mit therapeutisch interessanten Eigenschaften erhalten werden sollten.

Chemokine sind eine Gruppe kleiner, chemotaktischer Zytokine, die bei vielen physiologischen und pathologischen Vorgängen im menschlichen Körper beteiligt sind. Wegen ihrer wichtigen Rolle sind sie mit zahlreichen Krankheiten, vor allem mit Autoimmunerkrankungen und entzündlichen Erkrankungen wie chronischer Polyarthritid und COPD in Verbindung gebracht worden. Nachdem klar geworden war, dass die Einwanderung von Entzündungszellen in entzündete Herde durch die Interaktion von Chemokinen und Glykosaminoglykanen gesteuert wird, bietet dieser Mechanismus einen potentiellen Angriffspunkt für therapeutische Interventionen.

Dieser Weg würde die Einschränkungen und Probleme einer Therapie mit herkömmlichen Hemmstoffen (kleine organische Moleküle) und Antikörpern vermeiden.

ProtAffin ist eine Biotechnologiefirma, die das therapeutische Potential von Glykanbindenden Proteinen („decoy protein“) untersucht und bereits eine große Anzahl dominant-negativer Chemokin-Mutanten entwickelt hat. In den vorliegenden Untersuchungen wurde von der Arbeitshypothese ausgegangen, dass die Kombination modifizierter Chemokine in einem Molekül stärker wirksam ist als die einzelnen Moleküle sind oder dass sie eine neuartige Wirkung entfaltet.

Sechs solcher bifunktionaler Chemokine wurden in ausreichender Ausbeute und Reinheit erhalten, um damit eine vollständige chemische und biophysikalische Charakterisierung durchführen zu können. Weitere Untersuchungen sind vorgesehen, um die biologische Wirkung in experimentellen Entzündungsmodellen zu testen.

### **3. INTRODUCTION**

The present thesis describes results of experiments with two modified chemokines.

#### **3.1 CHEMOKINES**

Chemokines stand for a large group of small cytokines. Their name is the result of their ability to induce chemotaxis or the directed movement of cells through a concentration gradient: chemotactic cytokines. The first chemokine to be characterized was Interleukin 8 (IL-8) in 1987 by several groups (1, 2). Nowadays there are about 50 known ligands, 18 standard receptors and 5 atypical receptors of the human chemokine family. In their monomeric form their molecular weight (MW) of the ligands ranges from 7-12 kDa, the receptors are about 40 kDa. It was found that chemokine genes tend to form specific clusters on certain chromosomal sites (3).

##### **3.1.1 CLASSIFICATION OF CHEMOKINES**

Chemokines can be grouped into 4 different sub-categories according to their structure; more precisely on grounds of the highly conserved alignment of four cysteine residues (4). Between the four cysteines, two intramolecular disulphide bonds are formed between the first and the third cysteine and between the second and fourth cysteine, who form a typical greek key structure and give rise to the three dimensional structure. The CXC group (or  $\alpha$ -chemokine) is represented by chemokines who have their two N-terminal cysteines separated by one amino acid (X). CXC chemokine genes cluster on the chromosomal location 4q13.3. CXC chemokines can be further categorized into ones containing an ELR motif (Glu-Leu-Arg) that is located right before the first cysteine residue, and into ones lacking that specific motif (5). Chemokines containing the sequence (ELR+) are: CXCL1, CXCL2, CXCL3, CXCL5, CXCL6, CXCL7, CXCL8 (IL-8) and CXCL15. They are commonly angiogenic in character and possess the capacity of attracting neutrophils. The chemokines lacking the sequence (ELR-), CXCL4, CXCL9, CXCL10, CXCL11, CXCL12, CXCL13, CXCL14 and CXCL16 in contrast have angiostatic or anti-angiogenic properties and the ability to attract lymphocytes and monocytes. In contrast to the CXC group, the CC group (or  $\beta$ -chemokine) consists of chemokines who have two adjacent cysteines in the proximity of the N-terminus, for example CCL2 (MCP-1) or CCL5 (RANTES). CC chemokine genes are clustered on the location 17q12. The C group (or  $\gamma$ -chemokine) chemokines contain just two cysteines

and has only two known members, XCL1 and XCL2. These two chemokines only differ in 2 amino acids. The CX3C group (or  $\delta$ -chemokine) is the smallest as it has only one known member called Fractalkine who has 3 amino acids arranged between the first two cysteines and binds exclusively to CX3CR. Fractalkine is also the only known membrane bound chemokine so far, attached to the cell surface through a mucin like stalk. There is also a non-bound version of fractalkine with the ability to attract T cells and monocytes, whereas the membrane bound form seems to be involved into leukocyte adhesion (6, 7).

### **3.1.2 BASIC STRUCTURE**

All chemokines share a similar basic structure and a certain gene sequence homology. As a result the primary structure of chemokines differs from about 20% up to 90% in identity. The overall chemokine structure can be divided into 3 structural elements, first of all the flexible N-terminal domain before the first cysteine residue, than the first two cysteines are followed by the so called N-loop and further a  $3_{10}$  helix, three antiparallel beta-sheets and a C-terminal alpha helix (4, 6, 8).

### **3.1.3 CHEMOKINE RECEPTORS**

Chemokine receptors belong to the large superfamily of G-protein coupled receptors. More precisely chemokine receptors can be categorized as class A rhodopsin-like receptors, containing a characteristic 7 helical transmembrane structure with 3 intra and 3 extracellular loops. The N-terminus together with the 3 extracellular loops form the extracellular domain that is responsible for the ligand binding, whereas the C-terminus and the 3 intracellular loops form the intracellular domain that is responsible for signal transduction. Like their ligands, it is possible to categorize the receptors into 4 groups, CXCR, CCR, XCR and CX3CR. Binding of a chemokine ligand leads to activation of the receptor and further to diverse downstream events. (9)

### **3.1.4 CHEMOKINE FUNCTION**

The major function of chemokines is that of a chemoattractant. Chemokines have different roles to fulfill. For example there are chemokines who are in charge of the immune system and these so called homeostatic chemokines direct for example lymphocytes to the lymph nodes. Inflammatory chemokines are only secreted as a

response to viral or bacterial infection or physical cell damage as their main job is to recruit leukocytes to the center of inflammation or damage. Inflammatory CXC chemokines with a ELR sequence right before the first cysteine residue, have angiogenic properties in contrast to CXC chemokines lacking a ELR sequence (Glu-Leu-Arg) who are angiostatic (10). Chemokines are also crucial for development as they influence angiogenesis and embryogenesis.

### **3.2        THE ROLE OF CHEMOKINES IN PATHOLOGY**

Because of the major role chemokines play in intracellular signaling, inflammation and homeostasis they have been associated with the pathogenesis of many diseases, for example arthritis, systemic lupus erythematosus, multiple sclerosis, graft rejection and cancer (4, 11).

#### **3.2.1        *ROLE OF CHEMOKINES IN MULTIPLE SCLEROSIS (MS)***

“Multiple sclerosis is primarily an inflammatory disorder of the brain and spinal cord in which focal lymphocytic infiltration leads to damage of myelin and axons.” (12)

Multiple sclerosis is categorized as an autoimmune neuroinflammatory disorder, more precisely the disease is characterized by the infiltration of T-cells and macrophages into the periventricular region, causing lesions with damage to the axons. In the early stages of the disease, remyelination will occur after an exacerbation, thus reversing the damage and the symptoms to a certain extent. In the later stages the disease will switch over into the progressive form as the neurodegradation becomes chronic and irreversible (12, 13). Over the years MS has been extensively studied and it has become clear that cytokines and chemokines play an certain role in the pathogenesis of MS and other neuroinflammatory diseases, as they orchestrate the immune response and induce the chemotactic gradient required for the infiltration and accumulation of T-cells and further elevated levels of a number of chemokines has been found in serum and spinal fluid samples of patients. Together with other chemokines of the MCP family, MCP-1 or CCL2 is believed to play a major role in the etiopathology of multiple sclerosis. Utilizing immunohistochemistry and in situ hybridization McManus et al. (14) showed that MCP-1, MCP-2 and MCP-3 levels and activity are highly elevated in active lesions, whereas in

chronic plaques reactivity was reduced in human patients. On grounds of the influence chemokines and their receptors have on the immune response and inflammation, they are a promising target when it comes to finding a cure for MS or other neuroinflammatory or autoimmune diseases. However, it is still not fully established to which extent chemokines are involved in the pathogenesis of MS and their specific roles in the fragile signaling network.

### **3.2.2      *ROLE OF CHEMOKINES IN ARTHRITIS***

Arthritis is a multiform inflammatory disorder affecting the joints. Besides the most common form, osteoarthritis, which is mostly caused by age-related degeneration of the joints, there are also autoimmune forms like rheumatoid arthritis (RA). In RA leukocytes and monocytes break into the synovium of a joint and accumulate, producing chemokines. A number of chemokines and receptors (CCL2 (MCP-1), CCL3, CCL4, CCL5, CCL20, CXCL8 (IL-8), CXCL9, CXCL10, CCR1, CCR2 and CCR5) are thought to be involved to some extent in the pathogenesis of RA. IL-8, RANTES and MCP-1 further aggravate the inflammation by aiding the recruitment of further inflammatory cells into the synovium. Hayashida et al. (15) proved that MCP-1 and IL-8 play a crucial role in the aggravation of the inflammation, as they are locally produced by synovial stromal cells and initiate the recruitment of macrophages. Ultimately the inflammation results in the irreversible destruction of the joint and the bone (4, 16). Szekanez et al. examined the serum and synovium levels of cytokines (TNF $\alpha$ , IL-1 $\beta$ , IL-6) and chemokines (MIP-1 $\alpha$  and the murine equivalent of human MCP-1) over a 47 day period in rats utilizing adjuvant induced arthritis (AIA) as a model for RA. The group determined that the cytokine and chemokine production was significantly increased in rats with AIA compared to the control rats and that the elevated levels are linked to the clinical symptoms of RA (17). Among all involved chemokines, IL-8 seems to play a more important role than other factors. In animal models IL-8 is shown to be capable of inducing arthritis after a single injection. The importance of IL-8 in RA is further underpinned by the finding that the levels are increased in the serum, the synovial tissue and fluid of the befallen joint (4, 18-20).

### **3.2.3      *ROLE OF CHEMOKINES IN COPD (CHRONIC OBSTRUCTIVE PULMONARY DISEASE)***

COPD is a progressive inflammatory disease of the lungs, characterized by an advancing limitation of the airflow accompanied by an abnormal inflammatory response to cigarette smoke, particulate matter, air pollution or gases. Apart from environmental risks, there seems to be a certain genetic disposition (21). In the past decade it became the fourth leading cause of death worldwide, according to WHO (22). It is further estimated, that COPD will become a leading cause of death in the next 10 years, overtaking cardiac diseases. As there is no cure available so far, apart from lung transplantation, treatment takes places symptomatically. Common treatment strategies are tobacco abstinence, long term supplemental oxygen, inhalative treatment with corticosteroids, bronchodilators and beta 2 agonists. The pathogenesis of COPD is still not fully understood, but it seems to include genetic disposition as well as environmental risk factors, especially smoking. The pathognomonic symptom of COPD is the gradual irreversible limitation of the airflow caused by thickening and scarring of the airways in response to the constant infiltration of inflammatory cells. The airflow limitation is further characterized by a declining FEV1 (forced expiratory volume in 1 minute) and further to insufficient emptying of the lungs upon expiration. Patients suffering from COPD experience exacerbations at some point that become more and more frequent with the increasing severity of the disease over the years. While mild exacerbations are easily controllable with an increased dose of prescribed medication, severe exacerbations require hospitalization (23, 24). Another cardinal symptom, the inflammation of the lung tissue, is characterized by the chemokine-mediated infiltration of macrophages and neutrophils. As inflammatory chemoattractants, a number of different chemokines play an important role in the pathogenesis of COPD, for example IL-8, MCP-1 and GRO $\alpha$ . MCP-1 is an important chemoattractant for monocytes, the precursors of macrophages who are mostly responsible for the inflammatory response in COPD (25). This and the fact that MCP-1 levels are increased in sputum samples of patients, emphasizes the importance of this chemokine in COPD. Like MCP-1, IL-8 levels were found to be increased in sputum samples of COPD patients and correlated with the severity of symptoms. As IL-8 production and secretion are increased in COPD patients in comparison to healthy smokers, it is very likely that IL-8 is an important factor in COPD pathogenesis (25).

With increasing numbers of COPD patients around the world, research in this field has intensified. Based on their involvement in inflammation, chemokines were placed more and more into the limelight. The development of a blocking antibody for IL-8 was not significantly successful, as there is more than one chemokine involved in COPD, effectively bypassing the inhibition of IL-8 (26). Another starting point for the development of an inflammatory treatment based on chemokines is the inhibition of CXCR2 as many of the chemokines involved in COPD act through this receptor. So far some antagonists are under development by pharmaceutical companies or already in phase one clinical trial (26-28).

### **3.2.4      *ROLE OF CHEMOKINES IN NEOPLASTIC PROCESSES***

Cancer is the general term for a vast variety of diseases, characterized by unnaturally fast cell proliferation and eventually invasion and dissemination into distant tissues. Although it was found that complex interactions of many chemokines are involved in all stages of cancer, especially in tumorigenesis and metastasis, their real influence on the pathogenesis and the course of disease is still not well understood (29). Chemokines in cancer are a mixed blessing, as they are capable of tumor growth suppression and triggering antitumor responses as well as creating various advantages for the tumor (7). For example, it is very likely that chemokines are able to corrupt the organisms' immune system in a way that allows the cancer cells to spread without triggering specific defense mechanisms by specifically attracting T<sub>H</sub>2 lymphocytes as seen in Hodgkin lymphoma or Kaposi's sarcoma (4, 7, 30). Further chemokines are a crucial factor when it comes to tumor growth and survival, as angiogenesis is mandatory for dimensions over 2 mm in diameter. As already mentioned in the above sections, CXC chemokines with an ELR sequence as well as some CC chemokines have angiogenic effects *in vivo*. Arenberg et al. (31) showed in an animal model for non small cell lung carcinoma (NSCLC) that the inhibition of IL-8 is able to significantly reduce the size of the tumor. In contrast to ELR+ chemokines, it is proven ELR- chemokines like repress angiogenesis and thus tumor growth *in vivo*. In particular CXCL10 levels in patients with lung cancer are inversely related to tumor progression (7, 32-35).

### 3.3 GLYCOSAMINGLYCANS (GAG)

GAGs are linear, negatively charged polysaccharides composed of repeating disaccharide building blocks, consisting of a uronic acid (e.g. D-glucuronic acid or L-iduronic acid) and an amino sugar (D-galactosamine or D-glucosamine) (36). The overall negative charge is responsible for the binding with the positively charged chemokines. GAGs display highly variable structures through the number of disaccharides involved, N- or O-sulfatation, epimerization of the glucuronic acid residue into iduronic acid and the conformation of the glycosidic bond. The overall charge of the polysaccharide is negative at physiological conditions, due to the deprotonation of all sulfate and carboxyl groups (36-38).

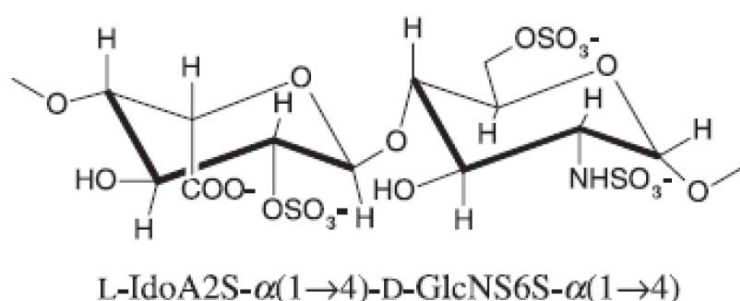


**Figure 1:** Structure of the major disaccharide repeating unit of heparin (38)

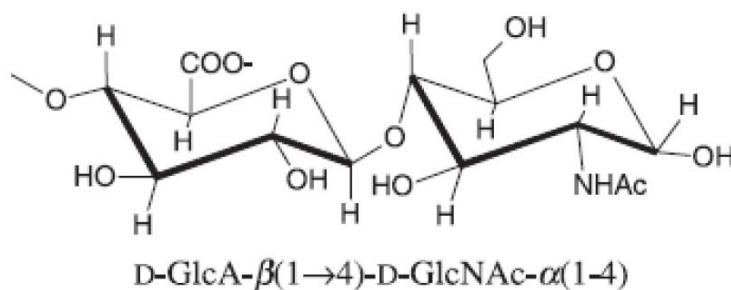


**Figure 2:** Structure of the major disaccharide repeating unit in heparan sulfate (38)

Until now, 6 classes of GAGs have been identified: heparin, heparan sulfate (HS), chondroitin sulfate (CS), dermatan sulfate (DS), keratan sulfate (KS) and hyaluronic acid (HA). GAGs are involved in a vast number of normal physiological but also pathological processes in the human body. For example wound healing, embryonic morphogenesis, general cell signaling through acting as co-receptors, angiogenesis, anti-coagulation, cancer metastasis and progression, microbial pathogenesis, Dengue fever, Alzheimer's disease, RA and Parkinson's disease. In consideration of the fact that

GAGs have been under extensive examination, heparin and heparan sulfate remain the most thoroughly investigated. As already mentioned above, GAGs play a significant clinical role. One of the most relevant functions discovered in 1917 would be the anticoagulant effect of heparin. It is used to treat and/or prevent deep vein thrombosis and embolism, through its ability to bind and activate antithrombin III (AT), the natural enzyme inhibitor of thrombin who is responsible for blood clotting (38).

### **3.3.1      *PROTEOGLYCANS (PG)***

PGs are macromolecules, expressed in nearly all mammalian cells, consisting of a core protein and one or more covalently bound GAGs. Their overall MW ranges from 10 kDa to more than 500 kDa. Under physiological conditions all GAGs with the exception of HA are covalently bound to a core protein. CS, HS, heparin and DS are bound through an O-glycosidic bond to a serine residue of the core protein, whereas KS is bound through a N-glycosidic bond to an asparagine residue on the core protein. The linker usually consists of a trisaccharide sequence with two galactose residues and one xylose residue (GAG-GalGalXyl-O-CH<sub>2</sub>-Protein).

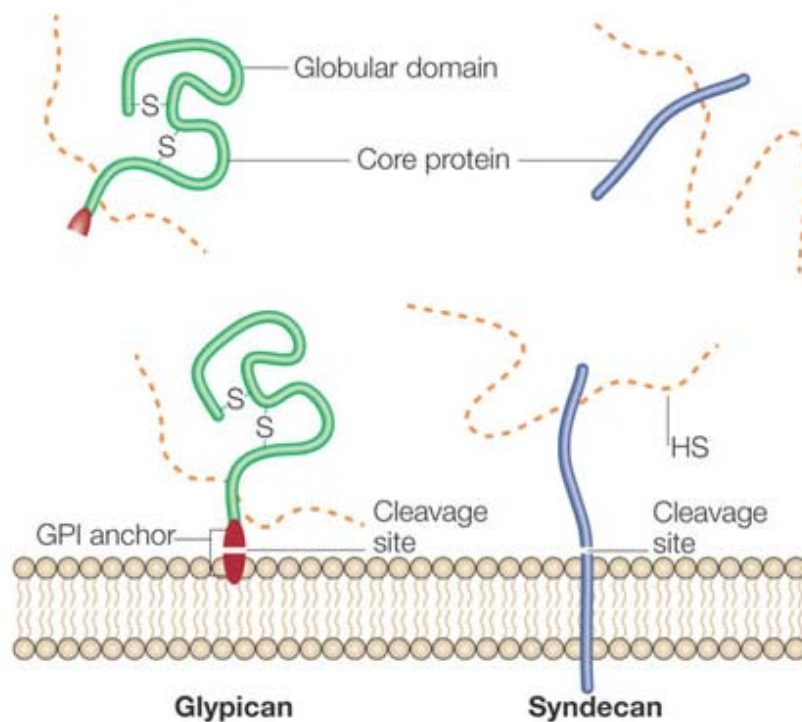
PGs are found in a vast number of structural varieties due to different core proteins and different substitution with GAG chains and are categorized according to the nature of the bound GAGs. The number of attached GAG chains also varies greatly, aggrecan for instance has more than 100 chains, whereas at the other side of the spectrum, glypicans carry only 1-3 chains (38, 39). Another fact that contributes to the complexity of PG structure is that one given PG can carry different GAG chains with different lengths and different arrangement of sulfated residues. (36, 38). Resulting from the structural diversity, it is not very surprising that they exhibit a vast array of different functions, for example structural organization of ECM and signal transduction.

Further, various proteins involved in different cell-matrix interactions (fibronectin), coagulation (AT III), inflammation (chemokines) and growth factors (FGF) use sulphated GAGs on PGs as co-receptors (36, 40-42).

Heparan sulfate proteoglycans (HSPG) are a type of PGs with a core protein and a varying number of HS chains attached to it. Studies suggest that HSPGs play a major role in both physiological and pathological processes, as they are heavily involved in signal transduction. HSPGs can be categorized into three groups according to their

localization (40, 43-45). However, the two major representatives of cell membrane HSPGs are syndecans and glypicans, their structure can be seen in Figure 3.

- ❖ membrane-spanning (e.g. syndecans, betaglycan)
- ❖ glycosylphosphatidylinositol (GPI)- linked (e.g. glypicans)
- ❖ extracellular matrix (ECM) (e.g. perlecan, agrin, collagen type XVIII)



Copyright © 2005 Nature Publishing Group  
Nature Reviews | Molecular Cell Biology

**Figure 3:** Structure of glypicans and syndecans (45)

### 3.3.2 CHEMOKINE - GAG INTERACTIONS

Nearly every known chemokine displays the ability to interact with GAGs, more precisely heparin and heparan sulfate. Further, the interaction with GAGs was proven to be crucial for the in vivo activity of several chemokines. The chemokine interaction with GAGs bound to the outer cell surface is thought to aid in the creation of a chemotactic gradient by immobilizing the chemokine and further the infiltration of leukocytes into the inflammation site by inducing chemotaxis (36, 38, 46, 47). The formation of the

chemokine gradient plays a major role in the clinical manifestation of an inflammation process, as the infiltration of inflammatory cells is crucial (48). Proudfoot et al.(49) demonstrated the significance of the chemokine/GAG interaction *in vivo* by showing that a chemokine with a genetically altered GAG binding site lose the ability to induce chemotaxis *in vivo*. Apart from their role in the gradient formation, it is estimated that the interaction may also have additional functions like the correct presentation of chemokines to their respective receptors or the protection from proteolytic cleavage (42, 47, 50, 51). Still, most of the specific chemokine/GAG interactions are not fully understood. Only in the last few years this field of research sparked the interest of the pharmaceutical research, as it became apparent in the course of the proteomics boom that these interactions pose a promising target for therapeutic intervention in many pathological processes (38, 49, 52).

### **3.4**        **DESCRIPTION OF MCP-1**

Monocyte chemoattractant protein 1 (MCP-1/CCL2) is categorized as a member of the CC chemokine family and was also the first one to be characterized in that group. MCP-1 is mainly secreted by monocytes but also by a variety of cell types. The structure determined by NMR resulted in 4  $\beta$  sheets and 2 helices, all together 76 amino acids (aa) in length and with a MW of 13 kDa. According to Meunier et al. (53) the secondary and quaternary structure of MCP-1 resembles the one of RANTES or MIP-1 $\beta$ . The genes encoding the receptor CCR2 are clustered on the chromosomal location 3p21-22. CCR2 binds all five pro-inflammatory members (CCL2, CCL7, CCL8, CCL12 and CCL13) of the MCP family, however binding of CCL2 triggers the strongest chemotactic signal. Further there have been 2 differently spliced forms of CCR2 identified; CCR2A and CCR2B. The sole difference between the two splice forms is made by the C-termini, although CCR2B seems to be the predominant isoform, as it is expressed in a much higher percentage than CCR2A. It is also estimated that the two isoforms trigger different signaling pathways upon activation. (8, 54) (Deshmane, Zlotnik).

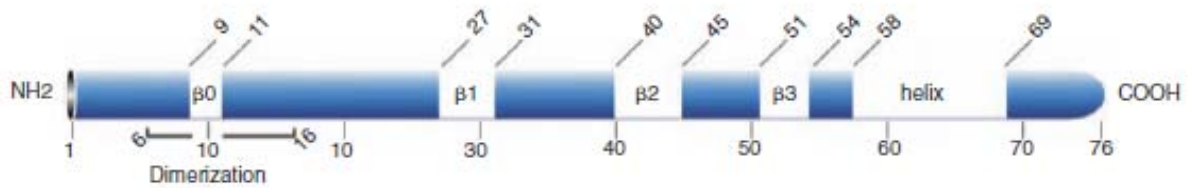


**Figure 4:** Shows the schematic representation of the CCL2 domain structure. (8)

In the case of MCP-1, it was demonstrated by Lau et al. that the oligomerization of MCP-1 in the presence of GAGs is crucial factor for the *in vivo* function. The residues Arg<sup>18</sup>, Arg<sup>24</sup>, Lys<sup>19</sup> and Lys<sup>49</sup> have been identified to play an important role in the interaction of MCP-1 and GAGs. (55)

PA508 is a MCP-1 mutant used in the generation of the first bifunctional series. The PA508 mutant was generated using ProtAffin's CellJammer™ technology, creating an engineered protein with an increased binding affinity to GAGs but impaired receptor binding to CCR2. Therefore, PA508 is not able to initiate the recruitment of monocytes and macrophages. Thus it reduces the overall infiltration of inflammatory cells to a center of inflammation resulting in a regression of the inflammation.

### **3.5 DESCRIPTION OF IL-8**

Interleukin 8 (IL-8/CXCL8) was one of the first chemokines to be discovered and characterized, originally from a culture of stimulated human blood monocytes. IL-8 belongs to the CXC ELR+ chemokine family and is mainly produced by macrophages, but also by endothelial cells, epithelial cells, fibroblasts, neutrophils etc. Its chemottractant activity mainly affects neutrophils, mediating the inflammatory response. IL-8 binds to 2 chemokine receptors, CXCR1 and CXCR2, whereas CXCR1 shows a higher affinity (56). The structure determined by NMR and X-ray crystallography revealed that human IL-8 forms homodimers, each monomer spanning 72 aa with a MW of 8.3 kDa (57). A 77 aa form of IL-8 has also been identified, which was found to be expressed in tissue cells like endothelial cells and fibroblasts, but the 72 aa variant is the predominant one (58).

PA401 is one of the two mutants used to generate the first series of bifunctionals. It is an IL-8 mutant, designed and generated by ProtAffin also using the CellJammer™

approach. It is currently the most advanced product, entering a phase 1 clinical trial in 2012 with respiratory diseases like COPD as main indication. PA401 displays an impaired receptor binding to CXCR1 and CXCR2 and an increased affinity to GAGs who are expressed on the cell surface, therefore preventing leukocyte recruitment and as a consequence inhibiting the initiation of inflammatory processes. (ProtAffin FactsSheet)

### **3.6**            **GLYCAN-BINDING DECOY PROTEINS - CELLJAMMER™**

The CellJammer™ is a discovery technology developed by ProtAffin Biotechnologie AG(59), aiming to generate novel protein drugs based on altered GAG binding mechanisms. By combining rational design, protein engineering and bioinformatics the Cell Jammer platform is able to create dominant negative mutants with an increased affinity to GAGs, impaired receptor binding. Using the IL-8 mutant as an example, upon deletion of the 6 N-terminal amino acids responsible for GSPR activation and introduction of basic amino acids in the C-terminal region to enhance GAG binding, the normal signaling pathway is interrupted, the chemotactic ability is deleted and the GAG affinity is increased, resulting in an anti-inflammatory behavior of the mutant (60).

## **4. MATERIALS AND METHODS**

All methods were performed according to ProtAffin standard operating procedures if not indicated otherwise.

### **4.2**            **CHEMICALS**

All chemicals, if not stated otherwise, were purchased from Sigma Aldrich.

25% Ammonia solution: Merck # K41339522

30% Dimethicone: Dow Corning Corporation # 0005955395

Acetate buffer, pH 4: GE # BR-1003-49

Acetonitrile for HPLC: Fisher # 10660131

Acetonitrile LiChroSolv: VWR # 1000302500

Amine-coupling Kit: GE # BR-1000-50

Benzonase: VWR # 1016540001

Bis-ANS: Molecular Probes, Invitrogen, # B-153  
Boric acid: Merck # 1-0177  
C1 chip: GE # BR-1005-40  
Cobalt chloride \* 6 H<sub>2</sub>O: Merck # C0484/C0557  
Copper (II) sulphate \* 5 H<sub>2</sub>O: Merck # C0495  
Ethanolamine: GE # 22-0526-52  
Ferrous sulphate \* 7 H<sub>2</sub>O: Merck # C1004  
Hydrochloric acid (25%): Merck # C1447  
Immun star Western C kit: Biorad # 170-5070  
Kanamycine: Sigma # K4000  
KH<sub>2</sub>PO<sub>4</sub>: Merck # A0134177013  
Mangan sulphate \* H<sub>2</sub>O: Merck # C2488  
MgSO<sub>4</sub>\*7H<sub>2</sub>O: Merck # K40451282013  
Na<sub>2</sub>HPO<sub>4</sub>: Merck # K40869776  
Neutravidin: Thermo # 31000  
Plastic vials d 11mm: GE # BR-1002-87  
Rubber caps type 2: GE # BR-1004-11  
SA chip: GE # BR-1000-32  
Sartopore 2 0.2 µm filter: Sartorius Stedim # 5445307H9 -- 00  
SeeBlue2 Plus Protein marker: Invitrogen # LC5925  
TOP10 and BL21 Star (DE3) Chemically competent cells: Invitrogen  
Water for HPLC: Fisher # 10449380  
Water for HPLC: VWR # 23595328  
Yeast extract: BD Bioscience # 0075798  
Zinc sulphate \* 7 H<sub>2</sub>O: Merck # C5009

#### **4.3**            **CHROMATOGRAPHY COLUMNS AND RESINS**

Butyl Sepharose 4 Fast flow: GE # 17-0980-01  
Fractogel EMD SO3- (M): VWR # 1168820100  
HiBar 250-25 cartridge filled with LiChrospher 100 RP-18 (12 µm): Merck # 1.50004 with  
# 119656 (customised filling)  
Macro-Prep High S Support: Biorad # 156-0030

#### **4.4**            **ANTIBODIES**

Anti-PA401 antibody 8A12\_B01 (rat, monoclonal); (Dr. E. Kremmer, Helmholtzzentrum)  
Anti-PA401 antibody 5F1 (rat, monoclonal); (Dr. E. Kremmer, Helmholtzzentrum)  
Anti-IL8 (H60) antibody (rabbit, polyclonal); (Santa Cruz: # sc-7922)  
Anti-IL8 (rabbit polyclonal, Dianova CYT-26672)  
Anti-MCP1 antibody (goat, polyclonal) (C-17); (Santa Cruz: # sc-1304)  
Anti-goat IgG-HRP (Sigma: # A5420)  
Goat anti-rat IgG-HRP (Jackson Immuno Research Labs / Dianova: # 112-035-003)  
Goat anti-rat IgG-HRP (Jackson Immuno Research Labs / Dianova: # 112-035-003)  
Goat anti-rabbit IgG-HRP (Jackson Immuno Research Labs / Dianova: # 111-035-003)  
Goat anti-rabbit IgG-HRP (Jackson Immuno Research Labs / Dianova: # 111-035-003)

#### **4.5**        **REFERENCE PROTEINS**

The reference proteins were prepared in house, different batches were used.

#### **4.6**        **GAGs**

LMW Heparin (Iduron, Batches BN1, BN3 and “3432”)  
Heparan sulfate (Iduron, Batch: BN1)  
Heparan sulfate (Celsus, HO-03103)

#### **4.7**        **CELL CULTURE**

*Cells:*

Neutrophils, freshly isolated

*Media:*

FBS Gold (PAA # A11-151)

DMEM (Sigma # D6546)

Penicillin/Streptomycin (Sigma P0781)

RPMI1640 (Sigma # R5886)

Stable glutamine 200 mM (PAA # M11-006)

Trypsin (0.25%)/EDTA (Sigma # T4049)

*Consumables, assay reagents and cell stains:*

3.0/5.0µm pore size, polycarbonate membrane; from Sigma Aldrich # 3398/3387.  
 FITC Dextran (Sigma # FD40S)  
 HBSS w/o Ca, Mg (PAA # H15-009)  
 Calcein AM (Sigma # 17783)  
 Calcein AM Red-Orange: (Invitrogen # C34851)  
 VybrantR DyeCycle™ Ruby stain (Invitrogen # V10309)

#### 4.8 BIFUNCTIONALS SEQUENCE OVERVIEW

The bifunctionals were purchased from DNA 2.0 in pJexpress411 vectors, optimized for expression in *E. Coli*. The plasmid contains a T7 promoter and kanamycine resistance.

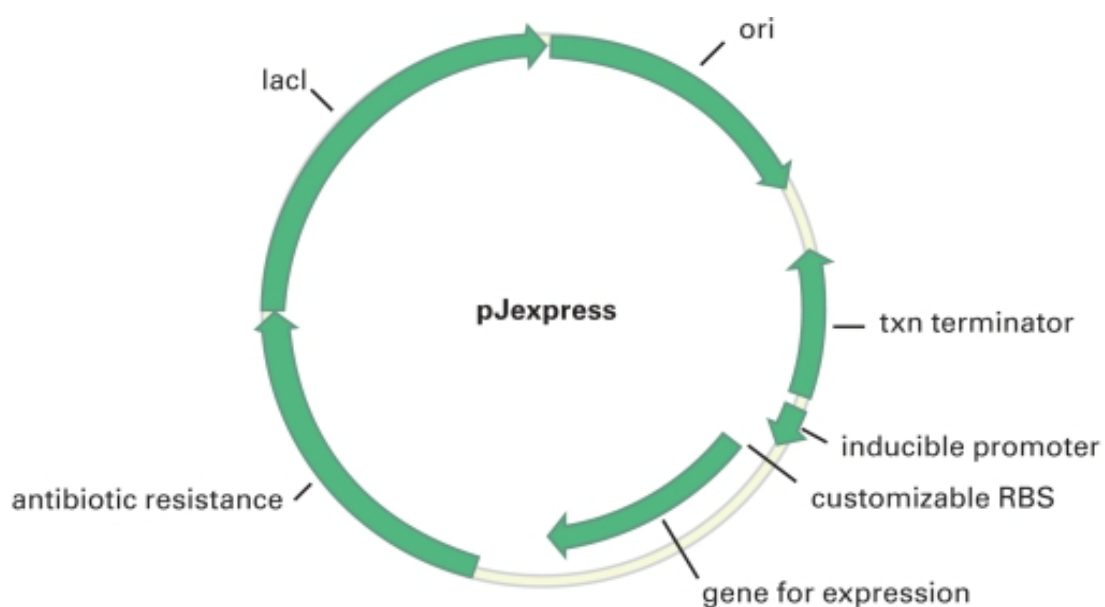


**Figure 5:** pJexpress411 vector from DNA2.0

The table below shows the six fusion proteins, composed of PA401 and PA508 in varying order and with different linker sequences.

**Table 1:** Overview of bifunctional protein sequences

<b>PA1113:</b> IL-8 [Δ6-F17K-F21K-E70K-N71K]-L1- MCP-1 [Y13A-S21K-Q23R-M64I]
<b>PA1114:</b> IL-8 [Δ6-F17K-F21K-E70K-N71K]-L2- MCP-1 [Y13A-S21K-Q23R-M64I]
<b>PA1115:</b> IL-8 [Δ6-F17K-F21K-E70K-N71K]-L3- MCP-1 [Y13A-S21K-Q23R-M64I]

**PA1116:** MCP-1 [Y13A-S21K-Q23R-M64I]–L1–IL-8 [ $\Delta$ 6-F17K-F21K-E70K-N71K]

**PA1117:** MCP-1 [Y13A-S21K-Q23R-M64I]–L2–IL-8 [ $\Delta$ 6-F17K-F21K-E70K-N71K]

**PA1118:** MCP-1 [Y13A-S21K-Q23R-M64I]–L3–IL-8 [ $\Delta$ 6-F17K-F21K-E70K-N71K]

**PA401 =** IL-8 [ $\Delta$ 6-F17K-F21K-E70K-N71K]

**PA508 =** MCP-1 [Met-Y13A-S21K-Q23R-M64I]

**L1 =** KPFHPKFIKE

**L2 =** PKFI

**L3 =** PASPASPAS

#### **4.9 FERMENTATION AND EXPRESSION ANALYSIS**

The shake flask expressions were performed by inoculation of 8 or 16 x 1 L LB medium containing 30  $\mu$ g/L kanamycin with 10 mL of ONC culture *E. coli* BL21 Star (DE3) per L of LB medium. The cells were grown to an OD<sub>600</sub> of 0.7-1 and induced with 0.4 or 1 mM IPTG (final. conc.). Cells were grown for 3 more hours and harvested by centrifugation at 7.000 x g for 10 min. The cell pellets were stored at -20°C for further analysis.

After induction with IPTG 1 mL samples of different flasks were collected for expression analysis.

OD<sub>600</sub> measurements were performed and the samples were centrifuged at 10.000 x g for 1 min. The pellets were resuspended in 100  $\mu$ l PBS and 100  $\mu$ l of FSB (2x) were added. The samples were sonicated and analysed by SDS-PAGE and subsequent Coomassie staining. The loading volume for of each sample was calculated as follows:

Concentration factor F = 10 (cell pellet from 1000  $\mu$ l culture resuspended in 100  $\mu$ l of buffer)

OD<sub>600</sub> at harvest x F = Z

❖ Volume to be loaded onto a 12-well gel: V = 270 $\mu$ l / Z

❖ Volume to be loaded onto an 18-well gel: V = 180 $\mu$ l / Z

## **4.10 PURIFICATION OF BIFUNCTIONAL PROTEINS (PA1113 – PA1118)**

### **4.10.1 CELL DISRUPTION, INCLUSION BODY (IB) SOLUBILISATION AND DIALYSIS**

The cell pellet was resuspended in a 4-fold volume of lysis buffer and stirred for 15 min at RT prior to sonication on ice at power level 6-7 for 6 x 20 s with 30 s breaks. The sample was centrifuged for 20 min at 20.000 g at 4°C and the supernatant discarded. The IB pellet was washed twice in IB wash buffer and subsequently centrifuged.

For the solubilisation of the proteins the IB pellet was resuspended in the 10-fold volume of solubilisation buffer and stirred for 3 h at RT prior to centrifugation at 20.000 g for 20 min at 4°C.

The solubilised proteins were refolded by dialysis against 10 L of refolding buffer. Dialysis was carried out in 3 steps for at least 2 h at 4°C (e.g. 2h dialysis at 4°C, buffer exchange, ONC dialysis at 4°C, buffer exchange, 2h dialysis at 4°C).

#### *Composition of lysis buffer:*

- ❖ 20mM Tris
- ❖ 50mM NaCl
- ❖ 1mM EDTA
- ❖ pH 8.0

#### *Composition of IB wash buffer:*

- ❖ 50mM Tris
- ❖ 100mM NaCl
- ❖ 10mM EDTA
- ❖ pH 8.0

#### *Composition of solubilisation buffer:*

- ❖ 10mM KH<sub>2</sub>PO<sub>4</sub>
- ❖ 6M Guanidine Hydrochloride (Gdn-HCl)

#### *Composition of refolding buffer:*

- ❖ 10mM KH<sub>2</sub>PO<sub>4</sub>
- ❖ pH 7.5

#### **4.10.2 1<sup>ST</sup> PURIFICATION STEP: CATION EXCHANGE CHROMATOGRAPHY**

After dialysis the resulting protein solution was centrifuged at 20.000 g for 20 min at 4°C. The sample was loaded onto a SP Sepharose column (SPFF) in buffer A (10 mM KH<sub>2</sub>PO<sub>4</sub> buffer, pH 7.5) with a flow rate of 10 mL/min. Subsequent elution was carried out using a linear gradient with an increasing NaCl concentration up to 1M in 10 CV and flow rate of 2 mL/min.

2 mL fractions were collected and analysis was performed by SDS-PAGE and Coomassie staining.

##### Mobile phase composition:

Buffer A:

- ❖ 10mM KH<sub>2</sub>P0<sub>4</sub>
- ❖ pH 7.5

Buffer B:

- ❖ 10mM KH<sub>2</sub>P0<sub>4</sub>
- ❖ pH 7.5
- ❖ 1M NaCl

#### **4.10.3 2<sup>ND</sup> PURIFICATION STEP: REVERSED PHASE HPLC**

Suitable fractions from the first chromatography step were selected and pooled on the basis of the performed gel analysis. The pooled fractions were used for the subsequent reversed phase (rp) HPLC purification step. The sample was adjusted to contain 10% acetonitrile (ACN) and 0.1% trifluoroacetic acid (TFA) prior to loading onto the column (LiChrosphere 100, RP-18, 10µm) in 10 % ACN, 0.1% TFA with a flow rate of 5 mL/min. Elution was carried out by application of the following gradient:

**Table 2:** Gradient used in the rpHPLC step

<b>Time [min]</b>	<b>% phase B</b>
5 min	0 % - 40%

20 min	40% - 60%
5 min	60 - 100%

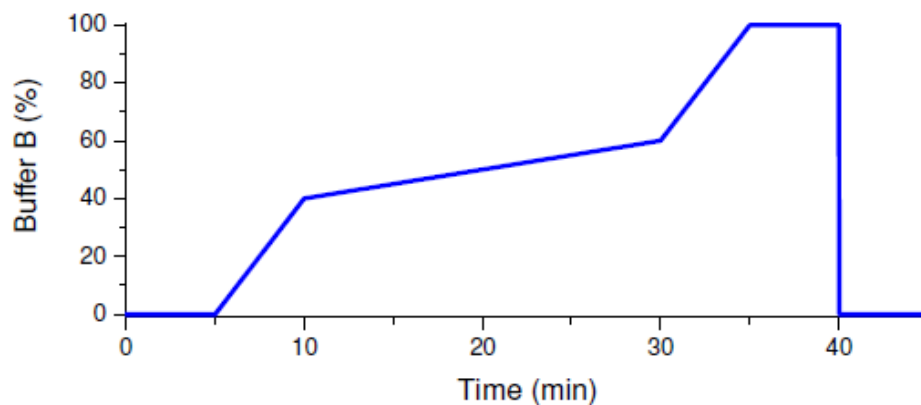


**Figure 6:** Graphic representation of the elution gradient.

10 mL fractions were collected and analysed by SDS-PAGE and subsequent Coomassie staining. The acetonitrile in the collected fractions was left to evaporate overnight in the fume hood.

Mobile phase composition:

*Phase A:*

- ❖ 10% ACN
- ❖ 0.1% TFA

*Phase B:*

- ❖ 90% ACN
- ❖ 0.1% TFA

**4.10.4 3<sup>RD</sup> PURIFICATION STEP: CATION EXCHANGE CHROMATOGRAPHY, REFOLD AND DIALYSIS**

The refold step was performed under “endotoxin-free” conditions using ddH<sub>2</sub>O (Fresenius), endotoxin-free reagents for buffer preparation and endotoxin-free tubes and tips. The SPFF column and the FPLC system were washed intensively with 1 M NaOH (min. 1h, 1 mL/min) prior to the run to remove endotoxins.

Suitable fractions were pooled and loaded onto the SPFF column in 10 mM KH<sub>2</sub>PO<sub>4</sub> buffer, pH 7.5 using a flow rate of 10 mL/min. Subsequent elution was carried out using a linear gradient with an increasing NaCl concentration up to 1M in 10 CV and flow rate of 2 mL/min.

2 mL fractions were collected and analysed by SDS-PAGE and Coomassie staining. Suitable fractions were pooled and concentrated if necessary using Amicon Ultra-4 filter devices (MWCO 3 kDa). Subsequent dialysis against PBS using Slide-A-Lyzers for 3 x 2h against 3 x 5 L of PBS at 4°C.

*PBS for dialysis:*

- ❖ 10 mM NaH<sub>2</sub>PO<sub>4</sub> \* 2 H<sub>2</sub>O
- ❖ 10 mM Na<sub>2</sub>HPO<sub>4</sub> \* 2 H<sub>2</sub>O
- ❖ 137 mM NaCl
- ❖ pH = 7.4

Mobile phase composition:

Buffer A:

- ❖ 10 mM KH<sub>2</sub>PO<sub>4</sub>
- ❖ pH 7.5

Buffer B:

- ❖ 10 mM KH<sub>2</sub>PO<sub>4</sub> buffer
- ❖ pH 7.5
- ❖ 1M NaCl

## **4.11 BIOPHYSICAL CHARACTERIZATION OF THE PURIFIED BIFUNCTIONAL PROTEINS**

### **4.11.1 DETERMINATION OF PROTEIN CONCENTRATION OF THE BIFUNCTIONALS**

The protein concentration was determined by measurement of the absorption at 280 nm (A280) and calculation of the protein concentration with the Lambert-Beer-Law using the theoretical coefficient of extinction (calculated with the ProtParam tool of ExPaSY). Either the Tray cell or the 100 µL cuvette was used.

#### **4.11.2 CONFIRMATION OF PURITY AND IDENTITY OF PURIFIED PROTEINS BY SDS PAGE (SODIUM DODECYL SULFATE POLYACRYLAMIDE GEL ELECTROPHORESIS)**

SDS Page is a technique that is used to separate proteins according to their electrophoretic mobility. SDS acts as a detergent, applying an overall negative charge on the protein, thus allowing a separation according to the size of the molecule (61).

The degree of contaminations of the purified proteins was determined by SDS-PAGE and subsequent Silver staining.

Additionally Western blots were performed to confirm the identity of the proteins. A number of different primary antibodies were used (see below) since some had not the ability to recognize all bifunctionals depending on the order of PA401 and PA506.

*Primary antibodies:*

- ❖ Anti-PA401 antibody 8A12\_B01 (rat, monoclonal)
- ❖ Anti-PA401 antibody 5F1
- ❖ Anti- IL-8 (H60) (Szabo Scandic)
- ❖ Anti- IL-8 (Dianova)
- ❖ Anti-MCP-1 antibody (goat, polyclonal) (C-17)

#### **4.11.3 CONFIRMATION OF IDENTITY AND QUALITY OF PURIFIED BIFUNCTIONALS BY MASS SPECTROMETRY**

The identification of the purified proteins was carried out by MS/MS by Dr.rer.nat. Gesselbauer at the department of pharmaceutical sciences at the Karl-Franzens University. For the analysis excised protein bands from a silver stained SDS-Page were used.

#### **4.11.4 LIMULUS AMEBOCYTE LYSATE (LAL) TEST**

The LAL test is used for endotoxin testing of substances that are intended for medical use for parenteral administration.

The experimental procedure for the LAL-Assay was performed according to the SOP. 3 different samples were prepared for each protein (50µg, 25µg, 16.7µg).

#### **4.11.5 DETERMINATION OF PROTEIN FOLD BY GUANIDINE UNFOLDING AND FLUORESCENCE SHIFT**

Guanidinium salts are used as a denaturing agent on proteins, where guanidine hydrochloride (Gdn-HCl) is one of the most effective ones. In a Gdn-HCl 6 M solution, all proteins are denaturated and obtain a random coil structure as the guanidine severs the intramolecular bonds and destroys their ordered secondary structure (62).

The protein samples were diluted to a final concentration of 700 nM in PBS or PBS containing 1/2/3/4/5/6 M Gdn-HCl. The samples were excited at a wavelength of 280nm and fluorescence emission spectra were recorded over the range of 300 - 400 nm on the Jasco FP-6500 fluorometer at 20°C.

**Table 3:** Settings for Record of Fluorescence Spectra

<b>Emission mode</b>
<b>Band width (Ex) 3 nm</b>
<b>Band width (Em) 3 nm</b>
<b>Response 1 sec</b>
<b>Sensitivity high</b>
<b>Auto shutter control on</b>
<b>Start 300 nm</b>
<b>End 400 nm</b>
<b>Ex-wavelength: 280 nm</b>
<b>Scan speed: 500 nm/min</b>
<b>Data pitch: 0,5 nm</b>

The fluorescence shift was determined by calculation of the ratios of the fluorescence intensities at 340 nm Flnt 340 divided by the Flnt 360 for the sample in PBS and in

denatured conditions (6 M Gdn-HCl). The fluorescence unfolding was evaluated by plotting the peak maxima (nm) against the concentration of Gdn-HCl and performance of a Boltzmann fit. The transition point of unfolding upon addition of chaotropic agent ( $x_0$ ) as well as the cooperativity of the curve ( $dx$ ) were determined.

#### 4.11.6 DETERMINATION OF SECONDARY STRUCTURE BY FAR-UV-CIRCULAR DICHROISM SPECTROSCOPY (CD SPECTROSCOPY)

CD spectroscopy uses the phenomenon that right-handed and left handed circularly polarized light is absorbed unequally after passage through an optically active sample. The far UV CD spectra of proteins are used to gain information on the secondary structure i.e. the proportion of  $\alpha$ -helices,  $\beta$ - sheets or random coil structures. Further, in our case this method is used to monitor changes in the secondary structure upon addition of GAGs, as the binding of a ligand induces a conformational change. (63)

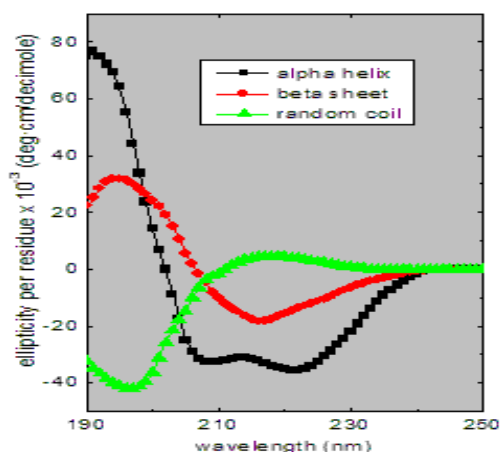


**Figure 7:** CD spectra standard obtained from [http://www.ap-lab.com/circular\\_dichroism.htm](http://www.ap-lab.com/circular_dichroism.htm)

All protein samples were diluted in PBS to a final concentration of 10  $\mu$ M and were analyzed without and with a 5-fold molar excess of GAG (Heparin Iduron BN3). The spectra were recorded from 250 nm to 190 nm using a quartz cuvette (Hellma, 165 QS 1mm). The following settings were applied:

**Table 4:** Settings for CD spectroscopy

<b>Sensitivity:</b> Standard (100 mdeg)
<b>Start wavelength:</b> 250 nm
<b>End wavelength:</b> 190 nm

<b>Data pitch:</b> 0.2 nm <b>Scanning mode:</b> continuous <b>Scan speed:</b> 50 nm/min <b>Response:</b> 1 second <b>Band width:</b> 1 nm <b>Accumulation:</b> 3
---

#### 4.11.7 DETERMINATION OF THE AFFINITY TO IMMOBILISED GAGs BY SURFACE PLASMON RESONANCE (SPR)

SPR based instruments utilize an optical method to measure changes in the refractive index near a sensor surface to study molecular adsorption and desorption events in real time. For interaction measurements, one interaction partner is immobilized onto the surface of the sensor and acts as the ligand. The other molecule of interest is dissolved into the sample buffer and injected into the flow cell. Upon binding to the ligand, the molecules accumulate on the sensor, causing a change of the refractive index that is proportional to the amount of bound analyte. The changes in the refractive index is recorded in real time and plotted as response units versus time in a so called sensorgram. SPR is a powerful method to determine the specificity of an interaction, the kinetics of an interaction, the binding affinity and the concentration of proteins (64, 65).

To investigate the affinity of PA1113-PA1118 to GAGs by SPR, different chips coated with heparin (Iduron BN1) were used. Namely a SA (carboxymethylated dextran pre-immobilized with streptavidin) chip and a C1 (carboxymethylated, matrix-free surface) chip, as some problems were encountered using the SA chip because of the high background. Following settings were used in the setup:

**Table 5:** SPR settings

Contact time: 120sec
Dissociation time: 120sec
Regeneration time: 60sec
Flow rate: 30 µl/min

**Table 6:** Bifunctional dilutions in PBST

Concentration	Volume
0	120 µl
50nM	200 µl
100nM	120 µl
250nM	120 µl

500nM	120 $\mu$ l
1000nM	120 $\mu$ l
1500nM	120 $\mu$ l

#### **4.11.8 DETERMINATION OF AFFINITY TO GAGs BY ISOTHERMAL FLUORESCENCE TITRATION (IFT)**

Isothermal fluorescence titration is a biophysical method based on the changes in the intrinsic fluorescence of folded proteins as a function of added ligand e.g. GAGs. It is used to monitor changes in the overall structure upon ligand binding or unfolding. The intrinsic protein fluorescence is due to the excitation of the aromatic residues of the amino acids tyrosine, phenylalanine but mostly tryptophan (61).

The IFT measurements were performed by automatic titration on the Fluoromax-4 Instrument (HORIBA Scientific) with an Automatic Titrator unit (Hamilton Microlab 500 series) using 250  $\mu$ L (injection-) and 1000  $\mu$ L (mixing-) syringes with end-tapered Teflon tubes. In preparation of the measurement, the samples were diluted to 700 nM in PBS in quartz cuvettes and equilibrated for about 30 min at RT. Measurements were carried out at a constant temperature of 20°C with 14 aliquots of the ligand injected into the cuvette (8 x 0.5  $\mu$ L and 6 x 1  $\mu$ L). The mixing syringe properties were: 150  $\mu$ L volume, 10 cycles every 60 seconds. LMW heparin (Iduron BN3; 250  $\mu$ M dilutions in dH<sub>2</sub>O) and HS (Iduron BN1; 250  $\mu$ M dilutions in dH<sub>2</sub>O) were used as GAG-ligands for the automatic titrations.

#### **4.11.9 DETERMINATION OF AFFINITY TO GAGs BY ISOTHERMAL TITRATION CALORIMETRY (ITC)**

ITC is used to measure the binding affinity of molecular interactions and all the thermodynamic parameters of the binding. It is a thermodynamic method based on the fact that upon binding of two molecules heat is either released or absorbed. The heat difference created by the reaction is measured in real time, thus allowing the determination of the reaction stoichiometry (n), the binding constants ( $K_B$ ), the reaction enthalpy ( $\Delta H$ ) and the entropy ( $\Delta S$ ) (61, 66).

15  $\mu\text{M}$  dilutions of purified proteins were prepared in PBS and titrated in the VP-ITC Microcalorimeter (MicroCal, LLC) adjusted with the Thermovac (MicroCal, LLC) with a 0.36 mM dilution of the ligand (GAG) in the same buffer. The parameters of the measurement are shown below:

**Table 7:** Isothermal Titration Calorimetry- Parameters

Cell temperature:	25°C
Reference power:	11.8
Initial delay:	60sec
Syringe concentration:	0.36mM
Cell concentration:	0.015mM
Stirring speed:	270
First injection:	2 $\mu\text{l}$
Following injections:	8 $\mu\text{l}$
Total number of injections:	38/25
Injection Volume:	2 $\mu\text{l}$ /8 $\mu\text{l}$
Injection Duration:	4/16 sec
Injection Spacing:	250 sec
Injection Filter period:	2

#### **4.11.10 DETERMINATION OF MW AND OLIGOMERISATION BEHAVIOUR BY SIZE EXCLUSION CHROMATOGRAPHY (SEC)**

Size exclusion chromatography is a chromatographic method where the analytes are separated by their size using the “molecular sieve” properties of porous column materials. The column material serves as the stationary phase, whereas the buffer serves as the mobile phase. When the sample is loaded evenly on the column material, the smaller particles are retained longer on the column material than the larger ones, thus separating the sample according to the size of the molecules of interest. This method is applied in particular on large molecules or complexes. (61, 67)

The size exclusion chromatography was performed on the Elite LaChrom HPLC (VWR) with a constant flow rate of 0.05 mL/min at RT. The columns used for the analysis were Superdex 75 PC3.2/30 (GE: # 17-0771-01) as well as the Superose 12 PC3.2/30 column (GE: # 17-0674-01).

#### **4.11.11 DETERMINATION OF MW AND OLIGOMERISATION BEHAVIOUR BY ANISOTROPY MEASUREMENTS**

Fluorescence anisotropy describes the phenomenon that upon excitation of the sample with polarized light the emitted light is also polarized. The extent of this polarization in ratio to the total light intensity is described as the anisotropy ( $r$ ) and the changes in polarization are measured. Anisotropy measurements provide information on the size of the molecule and the changes in size, the shape, the viscosity of the sample environment and protein ligand interactions and binding (68, 69).

In preparation for the measurement, the spectrofluorometer (Jasco FP-6500) was turned on 30 min prior. The water bath was adjusted to 20°C. The quartz cuvettes (stored in concentrated HNO<sub>3</sub>) were rinsed for at least 20 min with tap water then rinsed with dH<sub>2</sub>O and dried using a cuvette centrifuge. Dilutions of the bifunctionals were prepared in PBS and equilibrated for 20 min at 20°C (in the cuvettes in the water bath).

Spectrum measurements were carried out prior to the anisotropy measurements to determine the maximum emission wavelength for each protein with the settings described in Table 8 (in case of too high signal the Ex-slit was changed to 1 nm). Anisotropy measurements were performed in the „Fixed Wavelength Measurement“ mode with the settings shown in Table 8. The two polarisation filters („Filter 1“/“Ex“ and „Filter 2“/“Em“) were inserted into the instrument and measurements with the filter settings HEx/HEm, HEx/VEm, VEx/VEm and VEx/HEm were performed (“H” indicates horizontal polarised light, “V” stands for vertical polarised light and Ex and Em means “Excitation” and “Emission”).

**Table 8:** Settings for Anisotropy measurements

<b>Emission mode</b>
<b>Band width (Ex):</b> 3 nm
<b>Band width (Em):</b> 3 nm
<b>Response:</b> 1 sec
<b>Sensitivity:</b> high
<b>Auto shutter control:</b> on
<b>Excitation wavelength:</b> 280 nm
<b>Emission wavelength:</b> previously determined maximum emission wavelength
<b>Sample No.:</b> 1
<b>No. of cycle:</b> 5
<b>Cycle time:</b> 1 sec

*The G-factor and the anisotropy ( $r$ ) were calculated utilizing the following equations:*

$$G = \text{HexVem} / \text{HexHem}$$

$$\langle r \rangle = \frac{\text{Vex,Vem} - G \times \text{Vex,Hem}}{\text{Vex,Vem} + 2 \times G \times \text{Vex,Hem}}$$

#### **4.11.12 BOYDEN CHAMBER ASSAY**

Boyden chamber (chemotaxis) assays are experimental tools for evaluation of chemotactic ability of prokaryotic or eukaryotic cells. A wide variety of techniques are known and applied for such reason (70).

Boyden chamber assays were performed with three different cell types. Neutrophils were prepared freshly and the chemotaxis assay was performed. Monocytes were also isolated from fresh blood obtained from a healthy donor. A Neuroprobe 48-well chemotaxis chamber AP48, polycarbonate membrane with 5  $\mu\text{m}$  pore size: NeuroProbe # PFB5 was used.

## **5. RESULTS AND DISCUSSION**

All collected data belongs to ProAffin.

### **5.2 FERMENTATION AND EXPRESSION ANALYSIS**

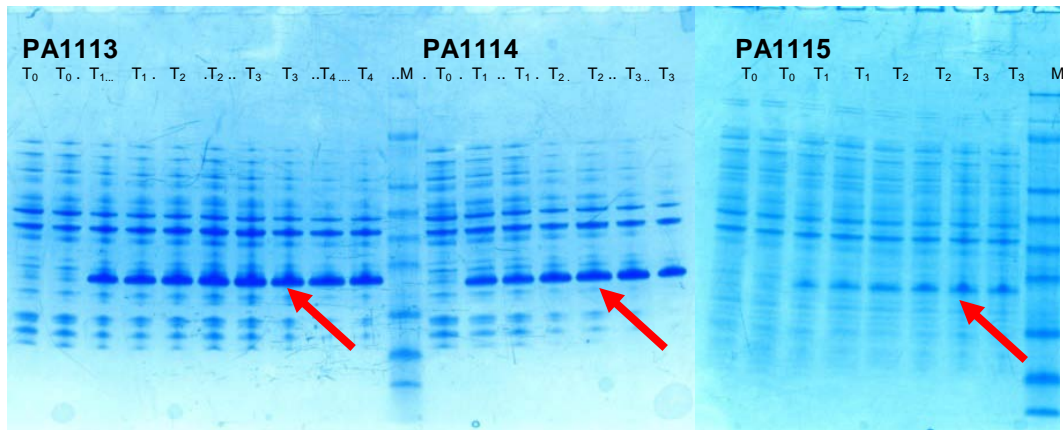


**Figure 8:** Expression analysis of PA1113 – PA1115 by SDS-PAGE and Coomassie staining before induction and after one to four hours. Red arrows indicating the anticipated protein band after induction of expression.

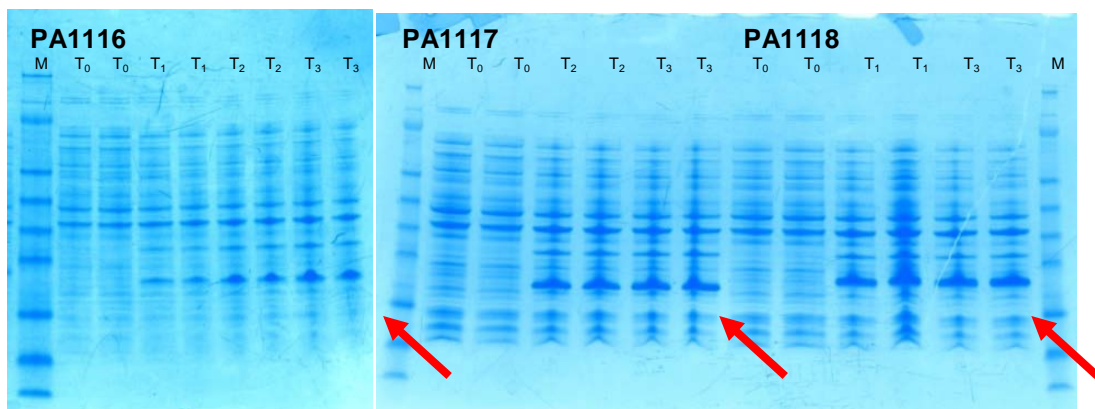


**Figure 9:** Expression analysis of PA1116-PA118 by SDS-PAGE and Coomassie staining before induction and after one to four hours. Red arrows indicating the anticipated protein band after induction of expression.

From the gel photos above we can see that the expression was successful overall, as the anticipated protein bands were visible in the samples after induction of protein expression with IPTG ( $T_{1-3}$ ) in contrast to the samples before induction ( $T_0$ ). The expression levels were average and remained unchanged throughout the fermentation.

### 5.3 PURIFICATION OF BIFUNCTIONAL PROTEINS (PA1113 – PA1118)

We purified the bifunctional series (PA1113 - PA1118) using standard chromatographic techniques in 3 steps. The first step was a FPLC cation exchange chromatography over a SPFF resin for pre-separation, followed by an rpHPLC step over a RP18 resin and a final FPLC cation exchange chromatography step over SPFF or another resin with

similar properties (e.g. MacroPrep). The results of the purifications are summarized below. For the first batches there was no optimized protocol available, the purification and refold conditions were roughly adopted from former purifications protocols for PA401, assuming that the fusion proteins would have a similar nature as the single mutants. Problems were encountered with the optimization of the protocol. In particular, the optimization of the refold step led to the generation of so called “sub-batches”, as we tried to find a way to decrease the amount of protein loss due to precipitation before the actual purification. We tried different approaches most notably shock dilution instead of dialysis and dilution of the sample before dialysis. Eventually the shock dilution was rejected due to the fact that it did not have the desired impact as it did not increase the protein yield significantly. Further it had the undesired side-effect of increasing the sample volume. Another problem we encountered was cross contamination of two batches PA1113 (B002) with PA1118 (B001) as later revealed by the MS/MS analysis. The resin of the reversed phase column was identified as underlying reason for the contamination. For this reason the rpHPLC step was later replaced by an FPLC step over a HIC resin for the purification of the successive bifunctional series.

#### **5.4        BIOPHYSICAL CHARACTERIZATION OF PROTEINS**

##### **5.4.1      *CONFIRMATION OF PURITY AND IDENTITY OF PURIFIED PROTEINS BY SDS-PAGE***

The SDS PAGE analysis and subsequent Silver staining confirmed the purity of the bifunctional products. The further confirm the identity a Western blot analysis was performed with an anti- IL-8 antibody.

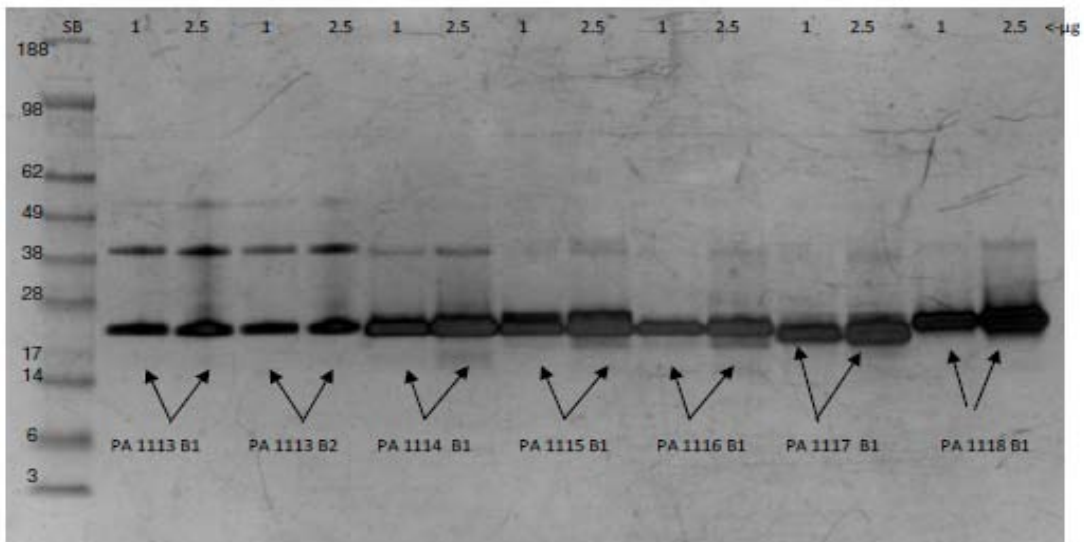


**Figure 10:** SDS PAGE analysis and Silver stain of purified bifunctionals PA1113 – PA1118.

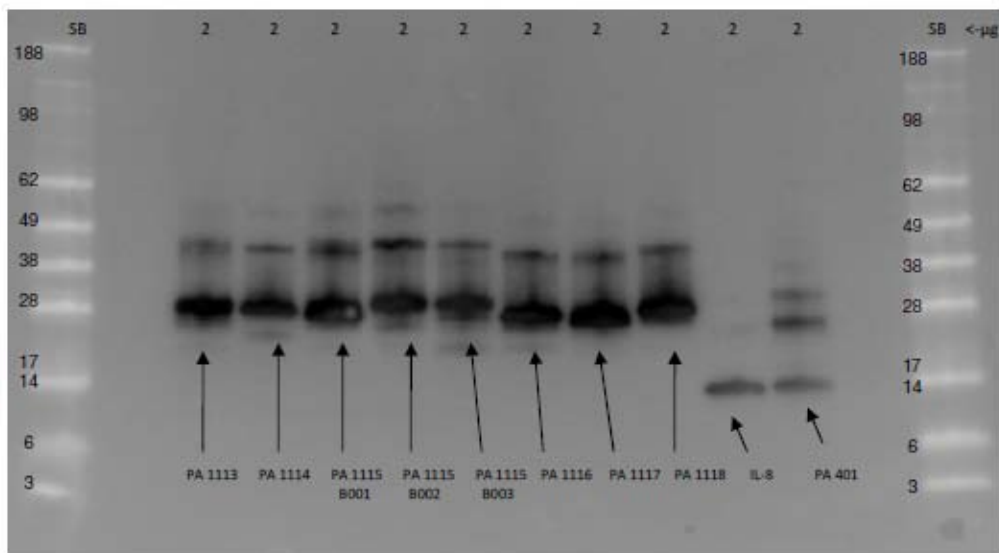


**Figure 11:** Western blot of purified bifunctionals PA1113 – PA1118 performed with IL-8 antibody (Szabo Scandic)

As there were several different primary antibodies available, all were tested in order to explore their detection limits. The anti-wT- IL-8 antibodies ((H-60) Szabo Scandic: # SC7922 and Dianova: # CYT-26672) were able to detect all bifunctionals. In contrast, the selective anti- PA401 antibody (8A12 and 5F1) only recognized the bifunctionals PA1116-PA1118 with PA401 in the C-terminus. Further the anti- MCP-1 antibody was also only able to recognize bifunctionals with the target sequence in the C-terminal part of the protein, therefore only PA1113-PA1115. Interestingly, the anti-MCP-1 antibody

was also able recognize the other bifunctionals with PA508 in the N-terminal part, but only to a very limited extent. This finding might be a further indication that the samples were slightly contaminated among each other, hence making the detection with anti-MCP-1 antibody possible.

#### **5.4.2 CONFIRMATION OF IDENTITY AND QUALITY OF PURIFIED BIFUNCTIONALS BY MASS SPECTROMETRY**

The spots of PA1113 – PA1118 excised from Silver stained gel were analysed by MS/MS. The spots of PA1114, PA1116, PA1117 and PA1118 could be clearly identified. For the PA1115 spot it was not possible to identify a characteristic peptide sequence, thus it is not possible to make a clear statement about the identity of the protein. In retrospect, it is not possible to attribute the measurement error with absolute certainty to neither a faulty excision of the protein spot nor to an insufficient amount of protein applied to the gel. However, the MS/MS analysis revealed a contamination of PA1113 (B002) with PA1118 (B001). We managed to retrace the contamination to the HPLC column used in the purification process. Apparently it was not possible to regenerate the column resin completely, even with a rigorous washing gradient.

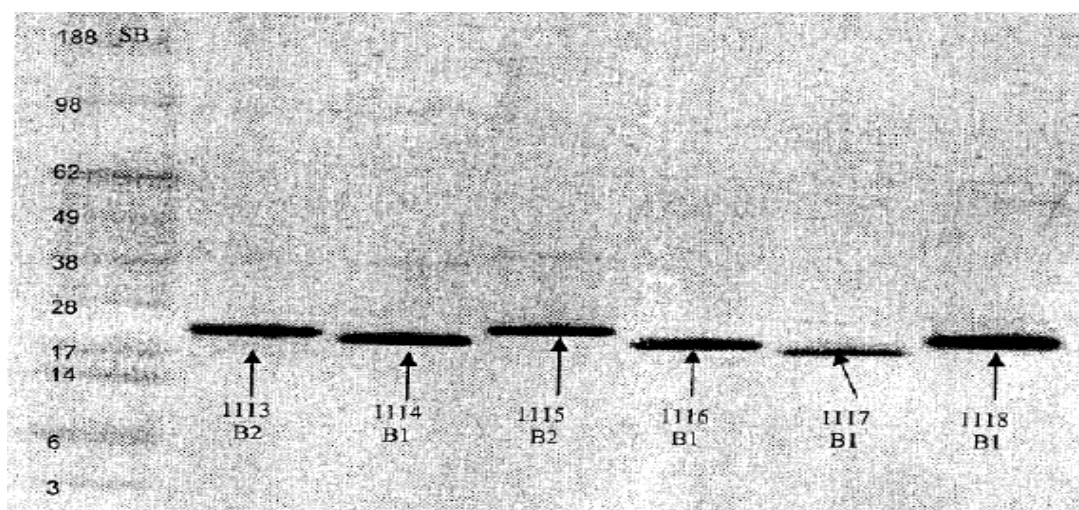


**Figure 12:** Silver stain of all 6 bifunctionals. The spots were excised and used for the MS/MS analysis.

**Table 9:** Summarized results of the MS/MS analysis (PA1113-PA1118)

Spot	Protein	Peptides Mascot	Spot	Protein	Peptides Mascot
1113_B2	PA1118	K.CPKEAVIFK.T K.WVQDSMDHLDK.Q K.TPASASPASCQCIK.T R.ELCLDPKENWVQR.V R.VIESGPHCANTEIVK.L K.WVQDSMDHLDKQTQPK.T -.MOPDAINAPVTCCANFTNR.K	1116_B1	PA1116	K.CPKEAVIFK.T K.EAVIFKTVAK.E K.FIKECCQIK.T K.WVQDSMDHLDK.Q R.ELCLDPKENWVQR.V R.VIESGPHCANTEIVK.L K.WVQDSMDHLDKQTQPK.T -.MOPDAINAPVTCCANFTNR.K -.MOPDAINAPVTCCANFTNR.I
	PA1113	K.CPKEAVIFK.T K.WVQDSMDHLDK.Q R.ELCLDPKENWVQR.V R.VIESGPHCANTEIVK.L K.WVQDSMDHLDKQTQPK.T K.EMQPDAINAPVTCCANFTNR.K K.EMQPDAINAPVTCCANFTNR.I	1117_B1	PA1117	K.EAVIFK.T K.FIQCCI.T K.TIVAKEICADPK.Q K.WVQDSMDHLDK.Q R.ITSSKCPKEAVIFK.T R.ELCLDPKENWVQR.V R.VIESGPHCANTEIVK.L K.WVQDSMDHLDKQTQPK.T -.MOPDAINAPVTCCANFTNR.K -.MOPDAINAPVTCCANFTNR.I
1114_B1	PA1114	K.CPKEAVIFK.T K.EAVIFKTVAK.E K.TIVAKEICADPK.Q K.WVQDSMDHLDK.Q R.ELCLDPKENWVQR.V R.VIESGPHCANTEIVK.L K.WVQDSMDHLDKQTQPK.T K.FIMQPDAINAPVTCCANFTNR.K	1118_B1	PA1118	K.EAVIFK.T K.CPKEAVIFK.T K.EAVIFKTVAK.E K.TIVAKEICADPK.Q K.WVQDSMDHLDK.Q K.TPASASPASCQCIK.T R.ELCLDPKENWVQR.V R.VIESGPHCANTEIVK.L -.MOPDAINAPVTCCANFTNR.K
1115_B2	???	K.CPKEAVIFK.T K.TIVAKEICADPK.Q R.ELCLDPKENWVQR.V R.VIESGPHCANTEIVK.L K.WVQDSMDHLDKQTQPK.T			

### 5.4.3 LIMULUS AMEBOCYTE LYSATE (LAL) TEST

LAL tests were performed on PA1113 B001/B002/B003, PA1114 B001, PA1115 B001/B003, PA1116 B001/B002, PA1117 B001/B002, PA1118 B001/B002. In all cases no or very low levels of endotoxins were detected.

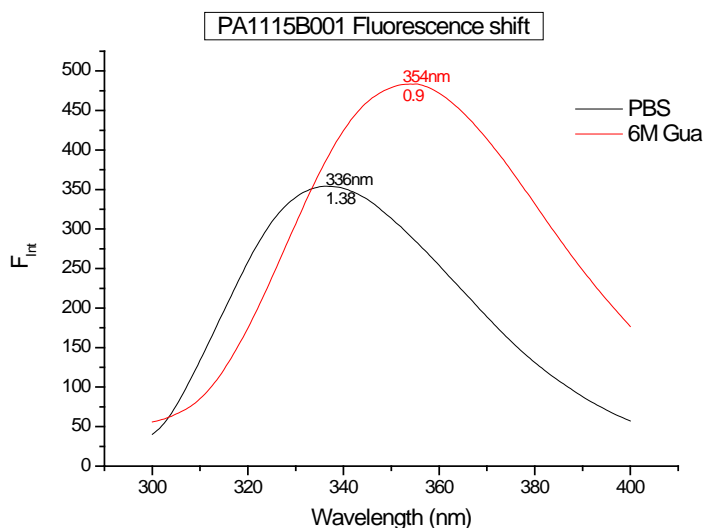
### 5.4.4 DETERMINATION OF PROTEIN FOLDING BY GUANIDINE UNFOLDING AND FLUORESCENCE SHIFT

In order to assess the folding of the protein samples, fluorescence shift and guanidine unfolding experiments were performed on all products and sub-batches. The results obtained from the fluorescence shift experiments are shown in Table 10. As can be seen from the table below, no significant differences in behavior were found between the bifunctionals or batches. The protein samples under physiological and under denatured conditions were examined at the excitation wavelength of 280 nm. The maximum emission wavelengths ( $\lambda_{max}$ ) in PBS ranged from 335.5 to 340 nm and shifted in a 6 M guanidine hydrochloride (Gdn-HCl) solution to a range of 353.5 to 354 nm. The significant shift in the emission maximum to higher wavelengths upon addition of the denaturing agent Gdn-HCl clearly demonstrates the unfolding of the protein. Figure 13Figure 5 provides an example of a fluorescence shift measurement.

**Table 10:** Results of all fluorescence shift experiments in PBS and in 6 M Gdn-HCl

Sample	$\lambda_{\max}$ PBS [nm]	FInt 340/360 PBS	$\lambda_{\max}$ 6M Gdn-HCl [nm]	FInt 340/360 6M Gdn-HCl
PA1113 B001	337.5	1.31	354	0.90
PA1113 B002	337	1.36	354.5	0.89
PA1113 B003	337	1.36	353.5	0.90
PA1114 B001	336	1.41	353	0.90
PA1115 B001	336	1.38	354	0.90
PA1115 B002	338	1.34	354	0.91
PA1115 B003	336.5	1.37	354	0.89
PA1115 B005	335.5	1.43	354	0.88
PA1115 B006	335.5	1.42	355	0.88
PA1115 B008	339	1.30	354.5	0.90
PA1116 B001	337	1.37	355	0.90
PA1116 B001	336.5	1.37	354	0.90
PA1116 B002a	338	1.33	354	0.91
PA1116 B002b	339.5	1.24	354	0.91
PA1117 B001	337	1.38	355	0.90
PA1117 B002a	339	1.30	354	0.91
PA1117 B002b	340	1.20	353	0.92
PA1118 B001	336	1.41	354	0.90
PA1118 B002	339	1.31	353.5	0.90

The results of the unfolding experiments are summarized in Table 11. As it can be seen from the data below, all tested proteins assumed an unfolded state upon the addition of Gdn-HCl to concentrations between 2.17M to 4.07M.

**Figure 13:** A fluorescence shift experiment using the example of PA1115 B001

**Table 11:** Result summary of the Gdn-HCl unfolding experiments

Sample	Transition point dx	Cooperativity of unfolding x0 [M]
PA1113B001	1,15	3,49
PA1113B002	0,76	3,27
PA1113B003	0,67	3,2
PA1114B001	0,66	4,07
PA1115B001	1,01	3,51
PA1115B002	0,87	3,66
PA1115B003	0,79	3,2
PA1115 B005	0,62	3,5
PA1115 B006	0,56	3,44
PA 1115 B008	0,73	3,42
PA1116B001	0,75	3,77
PA1116B001	0,56	3,1
PA1116B002a	0,63	3,1
PA1116B002b	0,97	2,3
PA1117B001	0,78	3,13
PA1117B002a	0,73	2,4
PA1117B002b	0,82	2,17
PA1118B001	0,48	3,85
PA1118B002	0,86	2,6

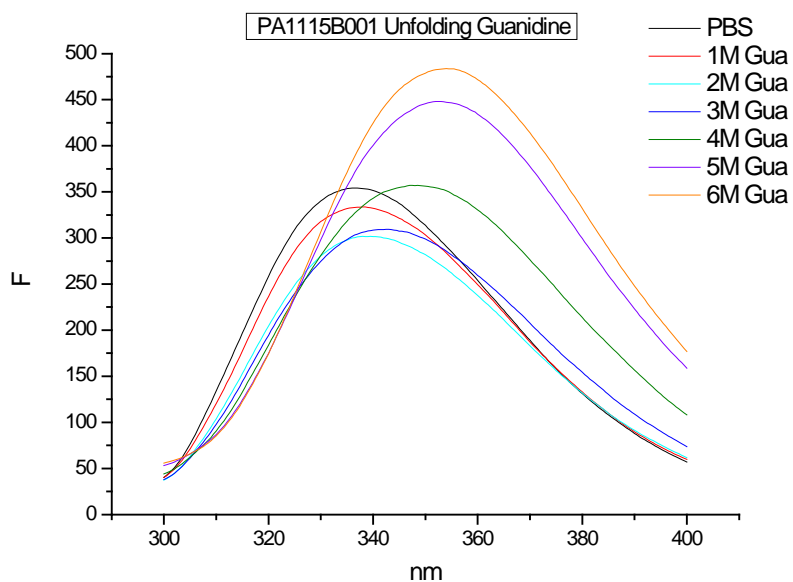


**Figure 14:** A fluorescence shift experiment using the example of PA1115 B001 with all concentrations

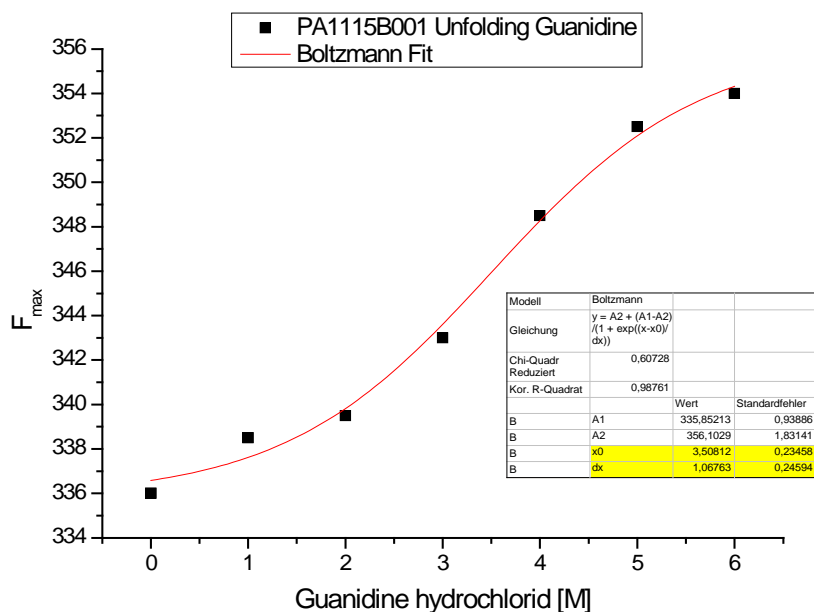


**Figure 15:** A guanidine unfolding experiment using the example of PA1115 B001

#### 5.4.5 DETERMINATION OF SECONDARY STRUCTURE BY FAR-UV-CIRCULAR DICHROISM SPECTROSCOPY (CD SPECTROSCOPY)

From the evaluation of the far-UV CD spectra it can be concluded that the bifunctionals are structured, at least to some degree, in the absence of GAGs as seen in figure 9. The addition of heparin (Iduron BN3) significantly decreased the signals, suggesting a change in structure or even precipitation in some samples as seen in figure 10. Overall, the results did not reveal any significant differences in structure among the samples, with the exception of PA1113. The experiment was repeated to exclude the possibility of a measurement error.

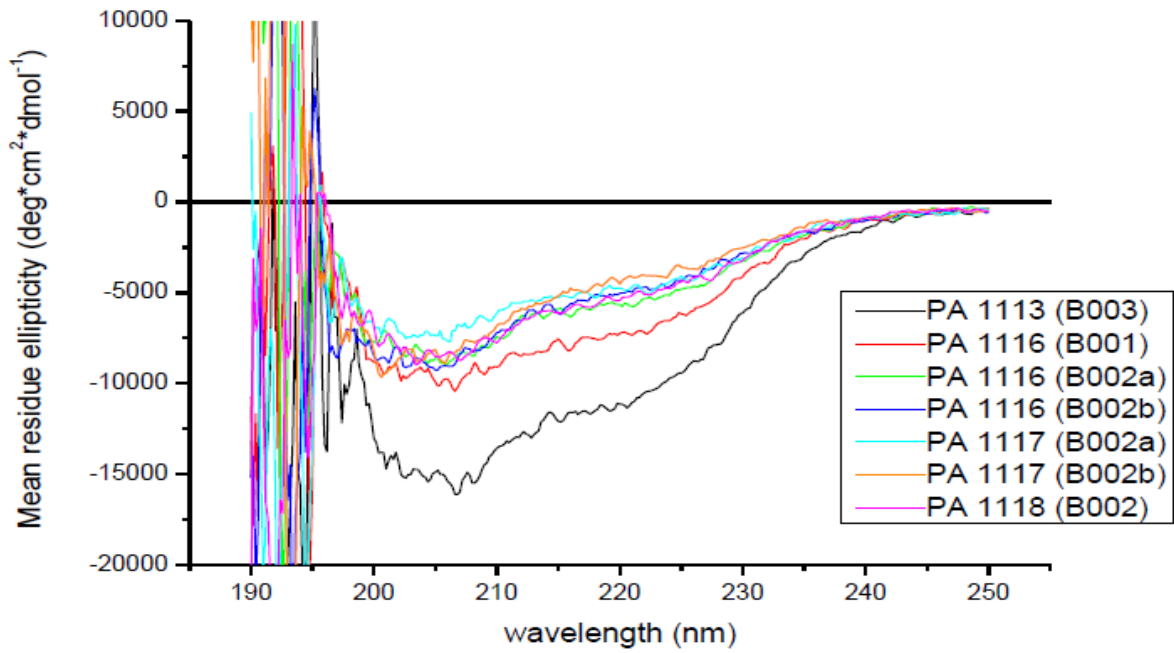


**Figure 16:** Overlay of the recorded spectra of PA113, PA1116, PA1117 and PA1118 in the absence of heparin

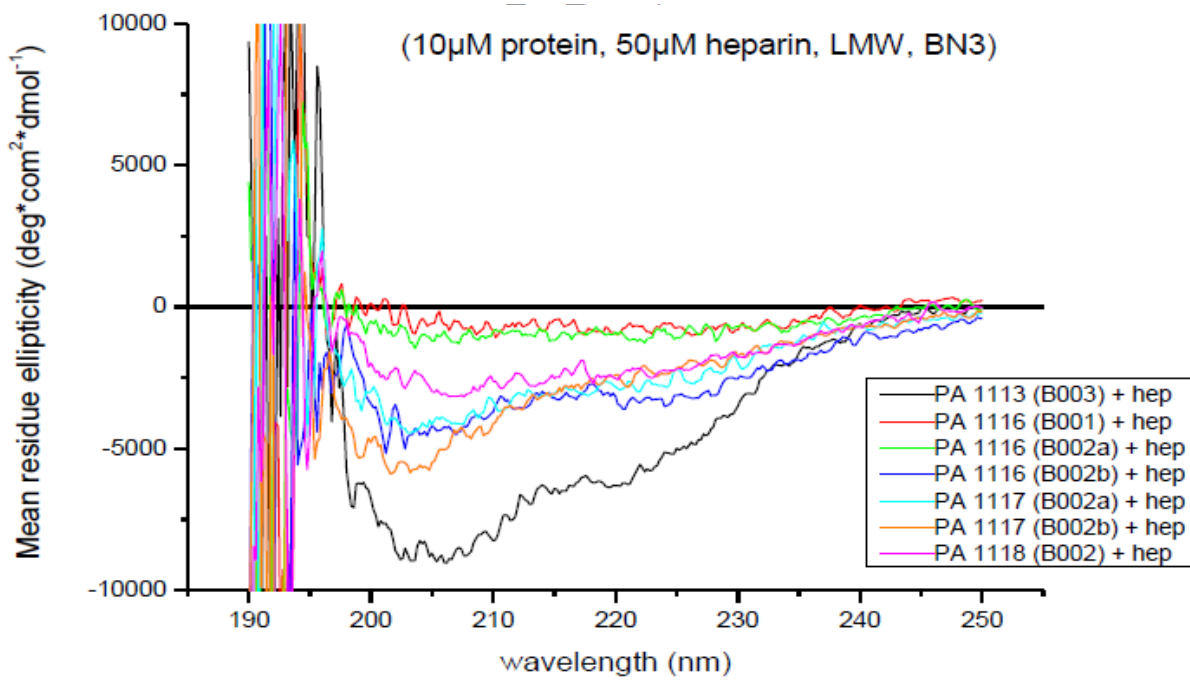


**Figure 17:** Overlay of the recorded spectra of PA113, PA1116, PA1117 and PA1118 in the presence of heparin

#### 5.4.6 DETERMINATION OF AFFINITY TO GAGS BY SURFACE PLASMON RESONANCE (SPR)

The tables 12 and 13 summarize the results obtained from the SPR analysis of PA1113-PA1118. Overall the bifunctionals showed a slightly higher or at least an equal affinity to heparin (Iduron BN3) than PA401. The data collected from the first measurement using a SA-chip turned out to be quite unreliable, because of the extremely high background signal. Especially the data of the measurements at lower concentrations were distorted by the high background, possibly creating delusive results. As anticipated, the background signal turned out to be significantly lower using the C1-chip, hence considerably improving the obtained data, as it is apparent from the  $\text{Chi}^2$  values in table 12.

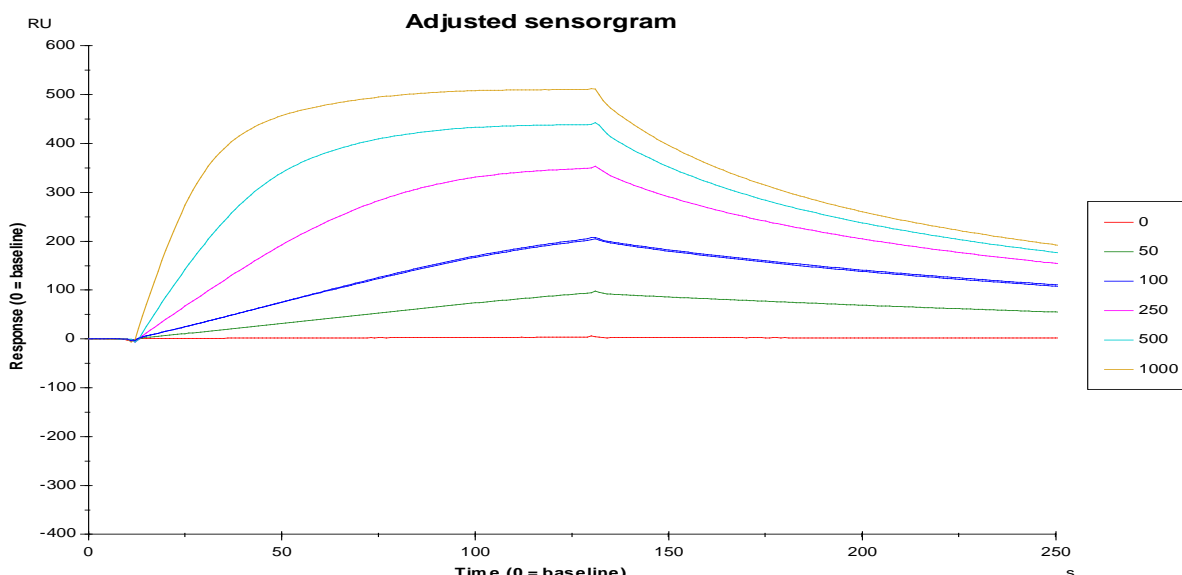


Figure 18: An exemplary sensorgram of PA401

Table 12: Results of measurements on a C1 chip

Protein	kD [nM]	Chi <sup>2</sup> [RU <sup>2</sup> ]
PA 1116(B001)	6.1	219
PA 1116(B002a)	263	593
PA 1116(B002b)	597	545
PA 1117(B001)	339	94.1
PA 1118(B001)	590	210

**Table 13:** Results of measurements on a SA-chip

<b>Protein</b>	<b>kD [nM]</b>	<b>Chi<sup>2</sup> [RU<sup>2</sup>]</b>
PA 401 LB 14	137 /146	18.5 / 4.1
PA 1113(B001)	337	1620
PA 1113(B002)	283	3220
PA 1114(B001)	41.9	8300
PA 1115(B001)	73	8430
PA 1116(B001)	41.9	6900
PA 1117(B001)	43.2	5060
PA 1118(B001)	62.3	8500

#### **5.4.7 DETERMINATION OF AFFINITY TO GAGs BY ISOTHERMAL FLUORESCENCE TITRATION (IFT)**

The results of the IFT measurements did not reveal any significant differences in affinity between the respective bifunctionals, as can be seen from the data summarized in table 14 and table 15. Apart from slight inconsistencies, the obtained results were overall in accordance with the results obtained from the preliminary SPR measurements. For testing purposes, measurements were carried using heparin as ligand for the titration, as well as heparan sulfate. However, the results as shown in the tables below indicate that there is no significant difference in affinity between heparin and heparan sulfate.

**Table 14:** Summarized results of all performed measurements with heparin (Iduron BN3) as ligand

<b>Sample</b>	<b>Kd [nM]</b>	<b><math>\sigma</math></b>
PA401ToxB0005	1175	83
PA401ToxB0005 DJ	947	152
PA508DS1117	1393	157
PA1113B002	440	57
PA1113B003	640	70
PA1114B001	458	34
PA1114B001	808	176
PA1115B001	466	63
PA1115B002	1059	63
PA1115B003	689	193
PA1115B002	788	36

PA1116B001	852	95
PA1116B002a	334	63
PA1116B002b	362	43
PA1116B001	518	83
PA1117B001	644	34
PA1117B002a	557	48
PA1118B001	538	39
PA1118B002	401	24
PA1118B001	549	35

**Table 15:** Summarized results of all performed measurements with heparan sulfate (Iduron BN1) as ligand

Sample	Kd [nM]	$\sigma$
PA1113B002	778	68
PA1114B001	573	65
PA1115B002	540	52
PA1116B001	1332	181
PA1116B002a	1435	96
PA1116B002b	588	165
PA1117B001	761	39
PA1117B002a	301	52
PA1118B001	254	28
PA1118B002	280	79

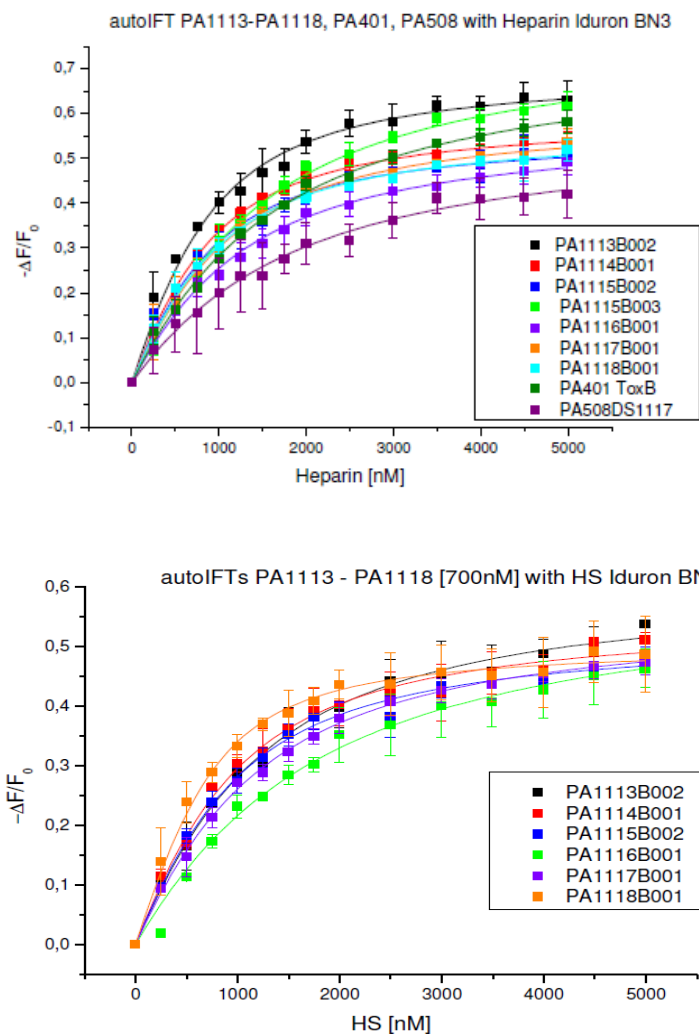


**Figure 19:** Overlay of all performed IFTs. The normalized change in fluorescence is plotted against the concentration of added ligand. The results of the titration with heparin are shown in the upper chart, whereas the results of the titration with heparan sulfate as ligand are shown in the lower chart.

#### 5.4.8 DETERMINATION OF AFFINITY TO GAGs BY ISOTHERMAL TITRATION CALORIMETRY (ITC)

Some problems were encountered while performing the ITC measurements, most notably sample precipitation and air bubbles were observed in some samples. Overall, the collected data further confirm the results obtained from SPR and IFT measurements, with the exception of PA1117 (B002) with a  $K_D$  value of 7600 nM. However the high  $K_D$  of PA1117 is most probably a runaway value caused by a measurement error.

**Table 16:** Summary of performed ITC measurements of PA1113-PA1118

Protein (7.5 $\mu$ M)	kD [nM]	N	Injections
PA 1113(B002)	138	0.66	25
PA 1114(B001)	1180	1.89	38
PA 1115(B002)	294	0.89	30
PA 1116(B002a)	990	1.34	30
PA 1116(B002b)	727	0.52	25
PA 1117(B001)	7600	0.001	25
PA 1118(B001)	1830	1.22	25

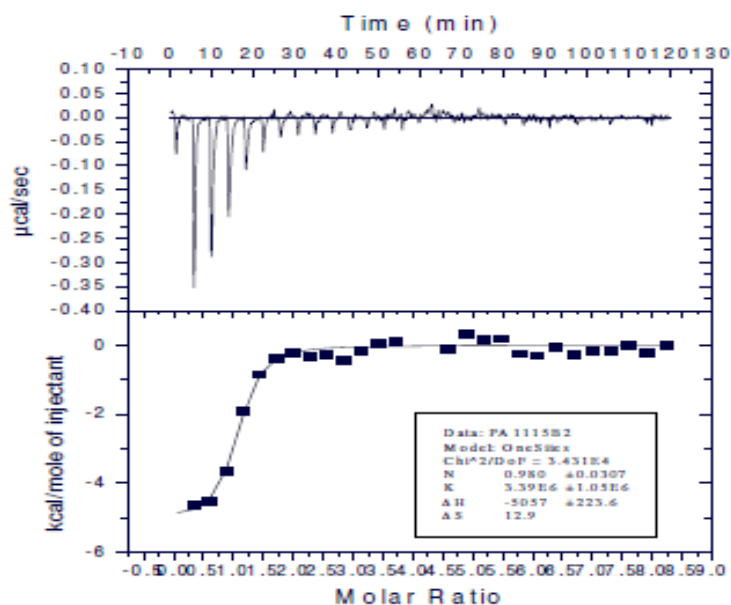


**Figure 20:** An exemplary ITC measurement showing the spikes in heat flow upon ligand injection in the upper part. The lower part shows the corresponding spectra after peak integration and plotted as a function of the molar ratio between the free ligand and the complex.

#### 5.4.9 DETERMINATION OF MW BY SIZE EXCLUSION CHROMATOGRAPHY (SEC)

The results for the SEC analysis are summarized in table 17. The experimental determination of the MW was overall successful with the exception of PA1113. No experimental data could be obtained for PA1113 as it was not possible to evaluate the recorded spectrum. Some problems have been encountered with the current set up, as the peaks did show moderate tailing. However, evaluation of the collected data was still possible and the experimental MW was determined. As it can be seen from table 17, the experimental data does not deviate significantly from the theoretical MW. Further the

SEC analysis showed that the bifunctionals assume a monomeric form under the present testing conditions.

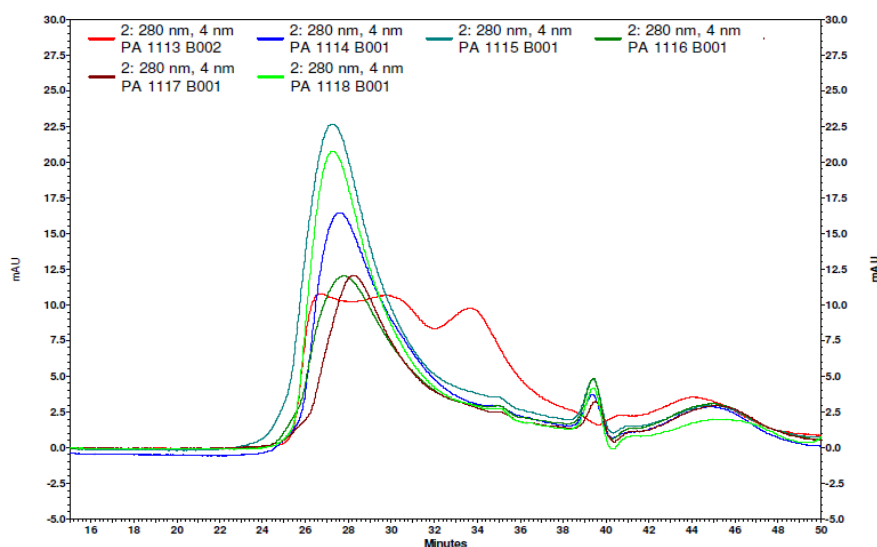


**Figure 21:** Summarized results of SEC analysis of PA1113-PA1118. The absorbance [mAU] is plotted against the retention time [min].

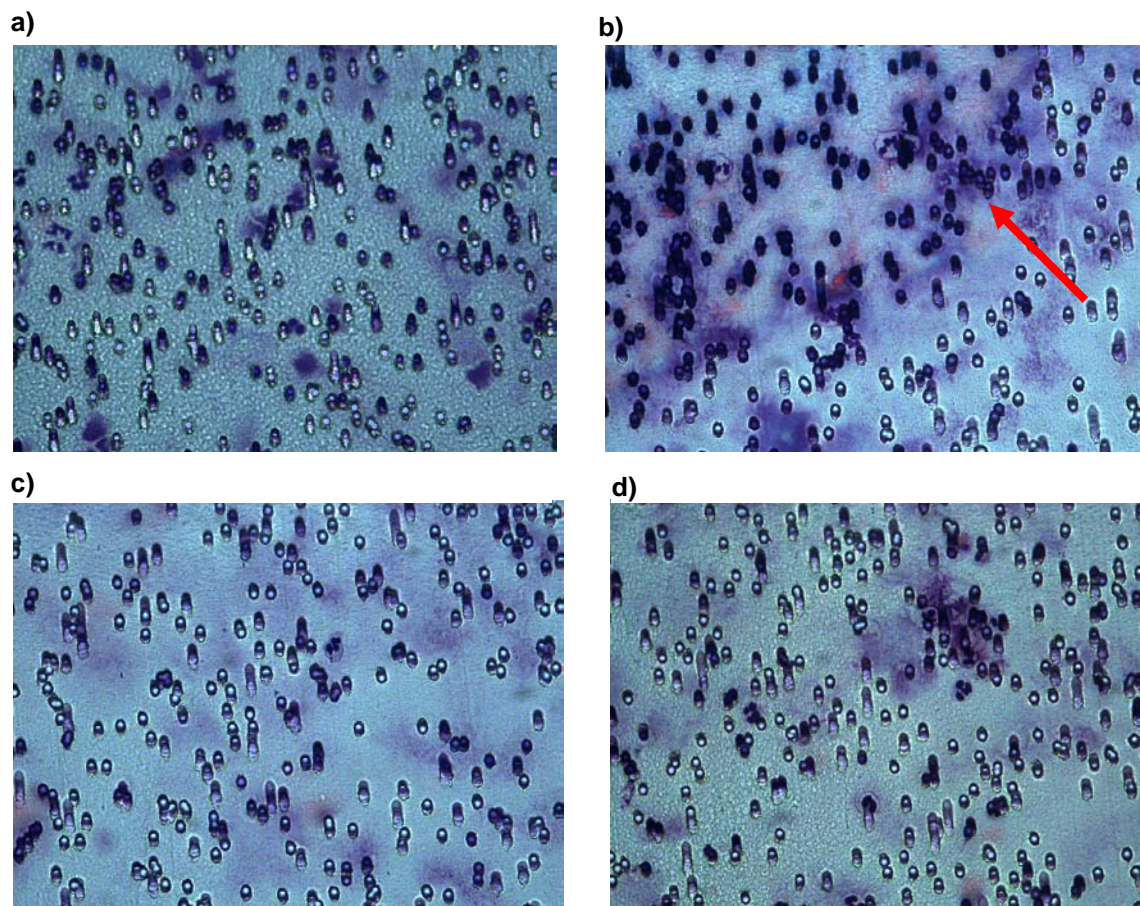
**Table 17:** Summarized results of the SEC analysis of PA1114-PA1118 as well as the calculated results for the MW.

Protein	Elution time [min]	Elution vol. [ml]	Experimental MW [kDa]	Theoretical MW [kDa]
PA 1114 (B001)	27.59	1.37	23.3	16.9
PA 1115 (B001)	27.27	1.36	25.5	17.2
PA 1116 (B001)	27.76	1.38	22.2	17.7
PA 1117 (B001)	28.20	1.41	19.6	16.9
PA 1118 (B001)	27.27	1.36	25.5	17.2

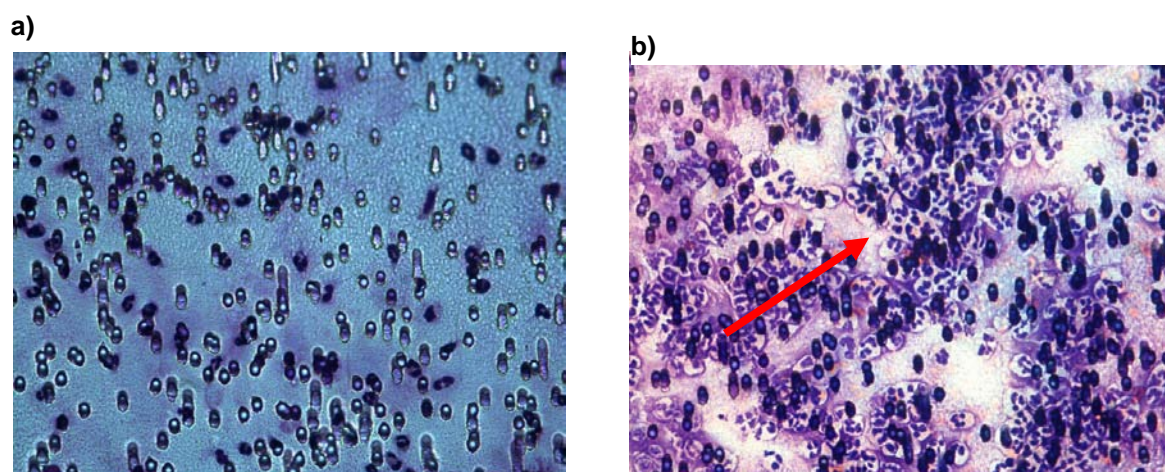
#### 5.4.10 BOYDEN CHAMBER ASSAY

A boyden chamber assay was performed for testing purposes with a single bifunctional (PA1115) and the IL-8 wt. The assay did not show any chemotactic ability of PA1115, as anticipated. Figure 16 shows representative pictures of the performed assay with the

bifunctional PA1115 applied in four increasing concentrations. Figure 17 shows pictures of the assay performed as a control with IL-8wt, again applied in four increasing concentrations.



**Figure 22:** Pictures of neutrophil cells after the performed boyden chamber assay. a) PA1115 13 nM b) PA1115 130 nM c) PA1115 1300 nM d) background with PBS



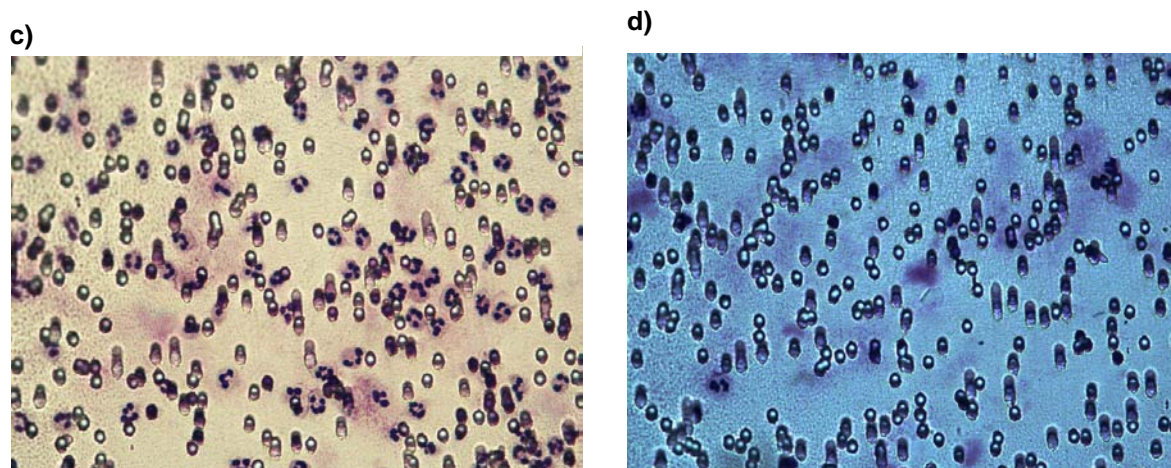


**Figure 23:** Pictures of neutrophil cells after the performed boyden chamber assay. a) IL-8 wt 13 nM b) IL-8 wt 130 nM c) IL-8 wt 1300 nM d) background with PBS

## 6. CONCLUSION

This project was undertaken to produce and characterize a novel type of a chemokine decoy protein based on PA401 and PA508. The current series of bifunctional chemokines was primarily thought to pose as a model for future fusion proteins based on other variants.

The results of this thesis show, that we succeeded to fulfill the aims set at the start of the thesis. We were able to express all 6 bifunctional variants in *E. coli*. The purification strategy had to be slightly optimized, however, we were able to obtain the desired proteins in satisfactory purity. Interestingly, one of the findings of the Western blot analysis was that the antibodies used in the analysis were only able to detect bifunctionals with the corresponding antigen in the C-terminal region of the protein. The subsequent MS/MS analysis clearly identified 5 of 6 bifunctionals, as for PA1115 it was not possible to identify any characteristic peptide sequence. However, the MS/MS analysis was able to pinpoint a weak spot in our purification strategy, what caused a cross contamination and was later identified as the reversed phase resin of the HPLC, as it was not possible to completely regenerate the column.

Taken together the results of the biophysical characterization experiments conducted to assess the affinity of the fusion proteins (IFT, ITC, SPR), were quite satisfactory. The

results suggest that the affinities of the bifunctional variants to GAGs (e.g. heparin, heparan sulfate) are higher or at least equal to wt MCP-1 and wt IL-8. The results of the CD analysis were very inconsistent as the measurements were limited by sample precipitation upon the addition of GAG, hence it was only possible to presume that there is a certain amount of secondary structure, but it was not possible to correctly analyze the obtained data. Another important finding was that the performed Boyden chamber assay was able to confirm the loss of chemotactic ability.

Finally, a number of important limitations need to be considered. First, these data only apply to fusion proteins composed of PA401 and PA508, two relatively well studied mutants. Second, problems were encountered while performing the CD and ITC analysis because of visible sample precipitation upon addition of ligand, especially at higher concentrations. More work will need to be done to get to the bottom of this phenomenon and to gain further insight into the actual structure. Third, the current project has only examined the chemotactic activity of one bifunctional protein, hence there are no data on the *in vivo* activity of the fusion proteins.

This project can serve as a base for future studies, as the methods used for this expression/purification/characterization may be used and optimized for new different bifunctional proteins composed of different fusion partners.

This research has thrown up many questions in need of further investigation. For example, contrary to our expectations, the affinities of the bifunctionals were not significantly higher compared to the single variants interaction.

Still, even without an increased affinity a fusion protein might be able to somehow combine the effects of the fusion partners by simultaneously antagonizing their respective receptors, thus creating a different effect and an advantage over the single variant.

## **7. REFERENCES**

1. Rollins BJ. Chemokines. *Blood*. 1997 Aug 1;90(3):909-28.
2. Yoshimura T, Matsushima K, Tanaka S, Robinson EA, Appella E, Oppenheim JJ, et al. Purification of a human monocyte-derived neutrophil chemotactic factor that has peptide sequence similarity to other host defense cytokines. *Proc Natl Acad Sci U S A*. 1987 Dec;84(24):9233-7.
3. Blanchet X, Langer M, Weber C, Koenen RR, von Hundelshausen P. Touch of chemokines. *Front Immunol*. 2012;3:175.
4. Bendall L. Chemokines and their receptors in disease. *Histol Histopathol*. 2005 Jul;20(3):907-26.
5. Vandercappellen J, Van Damme J, Struyf S. The role of CXC chemokines and their receptors in cancer. *Cancer Letters*. 2008;267(2):226-44.
6. Fernandez EJ, Lolis E. Structure, function, and inhibition of chemokines. *Annu Rev Pharmacol Toxicol*. 2002;42:469-99.
7. Locati M, Bonecchi R, Corsi MM. Chemokines and their receptors: roles in specific clinical conditions and measurement in the clinical laboratory. *Am J Clin Pathol*. 2005 Jun;123 Suppl:S82-95.
8. Deshmane SL, Kremlev S, Amini S, Sawaya BE. Monocyte chemoattractant protein-1 (MCP-1): an overview. *J Interferon Cytokine Res*. 2009 Jun;29(6):313-26.
9. Murdoch C, Finn A. Chemokine receptors and their role in inflammation and infectious diseases. *Blood*. 2000 May 15;95(10):3032-43.
10. Kiefer F, Siekmann AF. The role of chemokines and their receptors in angiogenesis. *Cell Mol Life Sci*. 2011 Sep;68(17):2811-30.
11. Luster AD, Alon R, von Andrian UH. Immune cell migration in inflammation: present and future therapeutic targets. *Nat Immunol*. 2005 Dec;6(12):1182-90.
12. Compston A, Coles A. Multiple sclerosis. *Lancet*. 2008 Oct 25;372(9648):1502-17.

13. Conductier G, Blondeau N, Guyon A, Nahon J-L, Rovère C. The role of monocyte chemoattractant protein MCP1/CCL2 in neuroinflammatory diseases. *Journal of Neuroimmunology*. 2010;224(1-2):93-100.
14. McManus C, Berman JW, Brett FM, Staunton H, Farrell M, Brosnan CF. MCP-1, MCP-2 and MCP-3 expression in multiple sclerosis lesions: an immunohistochemical and in situ hybridization study. *J Neuroimmunol*. 1998 Jun 1;86(1):20-9.
15. Hayashida K, Nanki T, Girschick H, Yavuz S, Ochi T, Lipsky PE. Synovial stromal cells from rheumatoid arthritis patients attract monocytes by producing MCP-1 and IL-8. *Arthritis Res*. 2001;3(2):118-26.
16. Klimiuk PA, Sierakowski S, Domyslawska I, Chwiecko J. Serum chemokines in patients with rheumatoid arthritis treated with etanercept. *Rheumatol Int*. 2011 Apr;31(4):457-61.
17. Szekanecz Z, Halloran MM, Volin MV, Woods JM, Strieter RM, Kenneth Haines G, 3rd, et al. Temporal expression of inflammatory cytokines and chemokines in rat adjuvant-induced arthritis. *Arthritis Rheum*. 2000 Jun;43(6):1266-77.
18. Endo H, Akahoshi T, Takagishi K, Kashiwazaki S, Matsushima K. Elevation of interleukin-8 (IL-8) levels in joint fluids of patients with rheumatoid arthritis and the induction by IL-8 of leukocyte infiltration and synovitis in rabbit joints. *Lymphokine Cytokine Res*. 1991 Aug;10(4):245-52.
19. Harada A, Sekido N, Akahoshi T, Wada T, Mukaida N, Matsushima K. Essential involvement of interleukin-8 (IL-8) in acute inflammation. *J Leukoc Biol*. 1994 Nov;56(5):559-64.
20. Szekanecz Z, Vegvari A, Szabo Z, Koch AE. Chemokines and chemokine receptors in arthritis. *Front Biosci (Schol Ed)*. 2010;2:153-67.
21. Dahl M, Nordestgaard BG. Markers of early disease and prognosis in COPD. *Int J Chron Obstruct Pulmon Dis*. 2009;4:157-67.
22. Decramer M, Janssens W, Miravittles M. Chronic obstructive pulmonary disease. *Lancet*. 2012 Apr 7;379(9823):1341-51.
23. Barnes PJ. The cytokine network in chronic obstructive pulmonary disease. *Am J Respir Cell Mol Biol*. 2009 Dec;41(6):631-8.
24. Kim V, Rogers TJ, Criner GJ. New Concepts in the Pathobiology of Chronic Obstructive Pulmonary Disease. *Proceedings of the American Thoracic Society*. 2008;5(4):478-85.

25. Traves SL, Donnelly LE. Chemokines and their receptors as targets for the treatment of COPD. *Current Respiratory Medicine Reviews*. 2005;1:15-32.
26. Barnes PJ. Future Treatments for Chronic Obstructive Pulmonary Disease and Its Comorbidities. *Proceedings of the American Thoracic Society*. 2008;5(8):857-64.
27. Barnes PJ. Are there any new therapies for chronic obstructive pulmonary disease? *US Respiratory Disease*. 2009.
28. Barnes PJ. New therapies for chronic obstructive pulmonary disease. *Med Princ Pract*. 2010;19(5):330-8.
29. Raman D, Sobolik-Delmaire T, Richmond A. Chemokines in health and disease. *Exp Cell Res*. 2011 Mar 10;317(5):575-89.
30. Skinnider BF, Mak TW. The role of cytokines in classical Hodgkin lymphoma. *Blood*. 2002 Jun 15;99(12):4283-97.
31. Arenberg DA, Kunkel SL, Polverini PJ, Glass M, Burdick MD, Strieter RM. Inhibition of interleukin-8 reduces tumorigenesis of human non-small cell lung cancer in SCID mice. *J Clin Invest*. 1996 Jun 15;97(12):2792-802.
32. Belperio JA, Keane MP, Arenberg DA, Addison CL, Ehlert JE, Burdick MD, et al. CXC chemokines in angiogenesis. *J Leukoc Biol*. 2000 Jul;68(1):1-8.
33. Liu M, Guo S, Stiles JK. The emerging role of CXCL10 in cancer (Review). *Oncol Lett*. 2011 Jul;2(4):583-9.
34. Strieter RM, Polverini PJ, Arenberg DA, Kunkel SL. The role of CXC chemokines as regulators of angiogenesis. *Shock*. 1995 Sep;4(3):155-60.
35. Strieter RM, Polverini PJ, Arenberg DA, Walz A, Opdenakker G, Van Damme J, et al. Role of C-X-C chemokines as regulators of angiogenesis in lung cancer. *J Leukoc Biol*. 1995 May;57(5):752-62.
36. Shute J. Glycosaminoglycan and chemokine/growth factor interactions. *Handb Exp Pharmacol*. 2012(207):307-24.
37. Mortier A, Van Damme J, Proost P. Overview of the mechanisms regulating chemokine activity and availability. *Immunology Letters*. 2012;145(1-2):2-9.

38. Gandhi NS, Mancera RL. The Structure of Glycosaminoglycans and their Interactions with Proteins. *Chemical Biology & Drug Design*. 2008;72(6):455-82.
39. Prydz K, Dalen KT. Synthesis and sorting of proteoglycans. *J Cell Sci*. 2000 Jan;113 Pt 2:193-205.
40. Perrimon N, Bernfield M. Cellular functions of proteoglycans--an overview. *Semin Cell Dev Biol*. 2001 Apr;12(2):65-7.
41. Hardingham TE, Fosang AJ. Proteoglycans: many forms and many functions. *FASEB J*. 1992 Feb 1;6(3):861-70.
42. Mulloy B, Rider CC. Cytokines and proteoglycans: an introductory overview. *Biochem Soc Trans*. 2006 Jun;34(Pt 3):409-13.
43. Baeg GH, Lin X, Khare N, Baumgartner S, Perrimon N. Heparan sulfate proteoglycans are critical for the organization of the extracellular distribution of Wingless. *Development*. 2001 Jan;128(1):87-94.
44. Bishop JR, Schuksz M, Esko JD. Heparan sulphate proteoglycans fine-tune mammalian physiology. *Nature*. 2007 Apr 26;446(7139):1030-7.
45. Häcker U, Nybakken K, Perrimon N. Developmental Cell Biology: Heparan sulphate proteoglycans: the sweet side of development. *Nature Reviews Molecular Cell Biology*. 2005;6(7):530-41.
46. Yu Y, Sweeney MD, Saad OM, Crown SE, Hsu AR, Handel TM, et al. Chemokine-glycosaminoglycan binding: specificity for CCR2 ligand binding to highly sulfated oligosaccharides using FTICR mass spectrometry. *J Biol Chem*. 2005 Sep 16;280(37):32200-8.
47. Johnson Z, Proudfoot AE, Handel TM. Interaction of chemokines and glycosaminoglycans: a new twist in the regulation of chemokine function with opportunities for therapeutic intervention. *Cytokine Growth Factor Rev*. 2005 Dec;16(6):625-36.
48. Taylor KR, Gallo RL. Glycosaminoglycans and their proteoglycans: host-associated molecular patterns for initiation and modulation of inflammation. *FASEB J*. 2006 Jan;20(1):9-22.
49. Proudfoot AE. The biological relevance of chemokine-proteoglycan interactions. *Biochem Soc Trans*. 2006 Jun;34(Pt 3):422-6.

50. Hoogewerf AJ, Kuschert GS, Proudfoot AE, Borlat F, Clark-Lewis I, Power CA, et al. Glycosaminoglycans mediate cell surface oligomerization of chemokines. *Biochemistry*. 1997 Nov 4;36(44):13570-8.
51. Kuschert GS, Hoogewerf AJ, Proudfoot AE, Chung CW, Cooke RM, Hubbard RE, et al. Identification of a glycosaminoglycan binding surface on human interleukin-8. *Biochemistry*. 1998 Aug 11;37(32):11193-201.
52. Rek A, Krenn E, Kungl AJ. Therapeutically targeting protein-glycan interactions. *British Journal of Pharmacology*. 2009;157(5):686-94.
53. Meunier S, Bernassau JM, Guillemot JC, Ferrara P, Darbon H. Determination of the three-dimensional structure of CC chemokine monocyte chemoattractant protein 3 by 1H two-dimensional NMR spectroscopy. *Biochemistry*. 1997 Apr 15;36(15):4412-22.
54. Zlotnik A, Yoshie O. Chemokines: a new classification system and their role in immunity. *Immunity*. 2000 Feb;12(2):121-7.
55. Lau EK, Paavola CD, Johnson Z, Gaudry JP, Geretti E, Borlat F, et al. Identification of the Glycosaminoglycan Binding Site of the CC Chemokine, MCP-1: IMPLICATIONS FOR STRUCTURE AND FUNCTION IN VIVO. *Journal of Biological Chemistry*. 2004;279(21):22294-305.
56. Hoch RC, Schraufstatter IU, Cochrane CG. In vivo, in vitro, and molecular aspects of interleukin-8 and the interleukin-8 receptors. *J Lab Clin Med*. 1996 Aug;128(2):134-45.
57. Baldwin ET, Weber IT, St Charles R, Xuan JC, Appella E, Yamada M, et al. Crystal structure of interleukin 8: symbiosis of NMR and crystallography. *Proc Natl Acad Sci U S A*. 1991 Jan 15;88(2):502-6.
58. Baggiolini M, Clark-Lewis I. Interleukin-8, a chemotactic and inflammatory cytokine. *FEBS Lett*. 1992 Jul 27;307(1):97-101.
59. Adage T, Piccinini AM, Falsone A, Trinker M, Robinson J, Gesslbauer B, et al. Structure-based design of decoy chemokines as a way to explore the pharmacological potential of glycosaminoglycans. *Br J Pharmacol*. 2012 Nov;167(6):1195-205.
60. Bedke J, Nelson PJ, Kiss E, Muenchmeier N, Rek A, Behnes CL, et al. A novel CXCL8 protein-based antagonist in acute experimental renal allograft damage. *Mol Immunol*. 2010 Feb;47(5):1047-57.

61. Lottspeich F, Engels JW. Bioanalytik: Spektrum Akademischer Verlag; 2006.
62. Seckler R, Jaenicke R. Protein folding and protein refolding. *FASEB J.* 1992 May;6(8):2545-52.
63. Bulheller BM, Rodger A, Hirst JD. Circular and linear dichroism of proteins. *Phys Chem Chem Phys.* 2007 May 7;9(17):2020-35.
64. N.N. Biocore sensor surface handbook. GE Healthcare.
65. Maynard JA, Lindquist NC, Sutherland JN, Lesuffleur A, Warrington AE, Rodriguez M, et al. Surface plasmon resonance for high-throughput ligand screening of membrane-bound proteins. *Biotechnol J.* 2009 Nov;4(11):1542-58.
66. Jelesarov I, Bosshard HR. Isothermal titration calorimetry and differential scanning calorimetry as complementary tools to investigate the energetics of biomolecular recognition. *J Mol Recognit.* 1999 Jan-Feb;12(1):3-18.
67. Kunji ER, Harding M, Butler PJ, Akamine P. Determination of the molecular mass and dimensions of membrane proteins by size exclusion chromatography. *Methods.* 2008 Oct;46(2):62-72.
68. Kapusta P. Time-resolved Fluorescence anisotropy measurements made simple: PicoQuant GmbH 2002.
69. Yengo CM, Berger CL. Fluorescence anisotropy and resonance energy transfer: powerful tools for measuring real time protein dynamics in a physiological environment. *Curr Opin Pharmacol.* 2010 Dec;10(6):731-7.
70. Pujic Z, Mortimer D, Feldner J, Goodhill GJ. Assays for eukaryotic cell chemotaxis. *Comb Chem High Throughput Screen.* 2009 Jul;12(6):580-8.